Mon. Not. R. Astron. Soc. **382,** 48–66 (2007) doi:10.1111/j.1365-2966.2007.12292.x

Wide-field mid-infrared and millimetre imaging of the high-redshift radio galaxy, 4C 41.17

T. R. Greve,[1⋆] D. Stern,[2] R. J. Ivison,[3,4] C. De Breuck,[5] A. Kovács[6] and F. Bertoldi[7]

[1]*California Institute of Technology, Pasadena, CA 91125, USA*
[2]*Jet Propulsion Laboratory, California Institute of Technology, Pasadena, CA 91109, USA*
[3]*UK Astronomy Technology Centre, Royal Observatory, Blackford Hill, Edinburgh EH9 3HJ*
[4]*Institute for Astronomy, University of Edinburgh, Blackford Hill, Edinburgh EH9 3HJ*
[5]*European Southern Observatory, Karl Schwarschild Strasse 2, D-85748 Garching bei München, Germany*
[6]*Max-Planck-Institut für Radioastronomie, Auf dem Hügel 69, 53121 Bonn, Germany*
[7]*Argelander Institute for Astronomy, University of Bonn, Auf dem Hügel 71, 53121 Bonn, Germany*

Accepted 2007 July 30. Received 2007 July 30; in original form 2007 June 4

ABSTRACT

We present deep 350- and 1200-μm imaging of the region around 4C 41.17 – one of the most-distant ($z = 3.792$) and luminous known radio galaxies – obtained with the Submillimeter High Angular Resolution Camera (SHARC-II) and the Max Planck Millimeter Bolometer Array (MAMBO). The radio galaxy is robustly detected at 350 and 1200 μm, as are two nearby 850-μm-selected galaxies; a third 850-μm source is detected at 350 μm and coincides with a $\sim 2\sigma$ feature in the 1200-μm map. Farther away from the radio galaxy additional nine sources are detected at 1200 μm, bringing the total number of detected (sub)millimetre-selected galaxies (SMGs) in this field to 14. Using radio images from the Very Large Array and *Spitzer* mid-infrared data, we find statistically robust radio and/or 24-μm counterparts to eight out of the 14 SMGs in the field around 4C 41.17. Follow-up spectroscopy with Keck/Low-Resolution and Imaging Spectrograph (LRIS) has yielded redshifts for three out of the eight robustly identified SMGs, placing them in the redshift range $0.5 \lesssim z \lesssim 2.7$ that is well below that of 4C 41.17. We infer photometric redshifts for a further four sources using their 1.6-μm (rest-frame) stellar feature as probed by the IRAC bands; only one of them is likely to be at the same redshift as 4C 41.17. Thus at least four, and as many as seven, of the SMGs within the 4C 41.17 field are physically unrelated to the radio galaxy. With the redshift information at hand, we are able to constrain the observed overdensities of SMGs within radial bins stretching to $R = 50$ and 100 arcsec (∼0.4 and ∼0.8 Mpc at $z \simeq 3.8$) from the radio galaxy to approximately five times and two times that of the field, dropping off to the background value at $R = 150$ arcsec. We thus confirm that 4C 41.17 resides in an overdense region of the Universe, but we have only been able to identify SMGs along the line of sight to the radio galaxy, typical of the blank-field SMG population. Finally, we report on the discovery of an extremely extended (∼110 kpc) Lyα blob at $z = 2.672$ associated with the brightest 1200-μm source in the field.

Key words: galaxies: formation – galaxies: individual: 4C 41.17 – galaxies: starburst – cosmology: observations – early Universe.

1 INTRODUCTION

Strong evidence has been unearthed by many independent studies, spanning the entire electromagnetic spectrum, that powerful ($P_{178\,\mathrm{MHz}} \gtrsim 10^{28}\,h^{-2}\,\mathrm{W\,Hz^{-1}}$) high-redshift ($z \gtrsim 2$) radio galaxies (HzRGs) are the progenitors of today's massive spheroids and giant ellipticals, seen in the early stages of their formation. Large radio luminosities indicate the presence of a supermassive black hole, while deep near-infrared (near-IR) observations betray large stellar masses, making HzRGs amongst the most-massive known baryonic systems in the distant Universe (e.g. Best, Longair & Röttgering 1998; De Breuck et al. 2002; Seymour et al. 2007). Another extreme property of HzRGs is the preponderance of luminous, morphologically complex Lyα haloes, extending up to 200 kpc from the central radio galaxies (e.g. Reuland et al. 2004). In

⋆E-mail: tgreve@submm.caltech.edu

several cases, strong H I absorption has been seen in Lyα, suggestive of vast reservoirs of neutral gas (e.g. Hippelein & Meisenheimer 1993; van Oijk et al. 1997; De Breuck et al. 2003; Wilman et al. 2004).

The first pointed submillimetre (submm) observations of HzRGs demonstrated that a large fraction of such systems are extremely luminous in the rest-frame far-IR waveband ($L_{\rm FIR} \sim 10^{13}\,{\rm L}_{\odot}$) and contain large amounts of dust ($M_{\rm d} \sim 10^{9}\,{\rm M}_{\odot}$ – Dunlop et al. 1994; Chini & Krügel 1994; Ivison 1995; Hughes, Dunlop & Rawlings 1997). Systematic 850-μm SCUBA surveys of HzRGs by Archibald et al. (2001) and Reuland et al. (2004) confirmed these initial findings and showed that the dust content of HzRGs, as gauged by the 850-μm luminosity, increases strongly with redshift: $L_{850\,\mu{\rm m}} \propto (1+z)^{3-4}$ out to $z \sim 4$. This was interpreted as a tendency for HzRGs to host younger stellar populations at higher redshifts since far-IR luminosities can be powered by either an active galactic nucleus (AGN) or starburst activity but large dust masses require vigorous recent star formation. Even though HzRGs undoubtedly host powerful AGN, starburst activity is therefore known to contribute substantially to their extreme far-IR luminosities; indeed, the lack of a correlation between radio power and submm luminosity seems to exclude a scenario in which the AGN are the dominating power source (Archibald et al. 2001). Furthermore, a handful of HzRGs are known to harbour large reservoirs of molecular gas ($M({\rm H}_2) \sim 10^{11}\,{\rm M}_{\odot}$ – e.g. Papadopoulos et al. 2000; De Breuck et al. 2003; Greve, Ivison & Papadopoulos 2004a; De Breuck et al. 2005; Klamer et al. 2005) – enough to fuel a $\sim$1000 $\,{\rm M}_{\odot}\,{\rm yr}^{-1}$ starburst for $\sim 10^{8}$ yr.

The environments of HzRGs are known to be extremely complex and to harbour a rich variety of galaxies. HzRGs are associated with overdensities of Lyα emitters (Venemans et al. 2007), Lyman break galaxies (Miley et al. 2004), Hα emitters (Kurk et al. 2003), extremely red objects (EROs – Kurk et al. 2004; Kodama et al. 2007), X-ray emitters (Pentericci et al. 2002; Smail et al. 2003b), as well as of dusty submm galaxies (Ivison et al. 2000; Smail et al. 2003a; De Breuck et al. 2004). One of the most-striking examples of the latter came from the first 850-μm SCUBA imaging of HzRGs (Ivison et al. 2000; Stevens et al. 2003). This revealed extended ($\sim$30 kpc) dust emission around the central radio galaxies and an apparent overdensity of SMGs (by a factor of 2 compared to blank-field surveys), suggestive of many vigorous starbursts occurring within a few Mpc of the central HzRGs.

These observational data all tally with current models of hierarchical structure formation, in which galaxy formation is anti-hierarchical and heavily biased towards regions of high density. The various source overdensities suggest that HzRGs are excellent markers of the densest and most-vigorous star-forming regions in the early Universe. HzRGs thus constitute an important population for benchmarking current models of galaxy formation, particularly at the high-mass end. The suitability of HzRGs for probing galaxy formation and evolution is furthered by the fact that HzRGs are (1) possible to identify in low-frequency radio surveys as ultrasteep-spectrum radio sources (Chambers et al. 1996; De Breuck et al. 2000) which, when combined with near-IR colour criteria, provide a highly efficient and relatively unbiased (in particular with respect to their dust properties) selection scheme, and (2) have accurate radio positions and extreme properties (e.g. large rest-frame optical luminosities) which aid their study.

In this paper, we present 1200- and 350-μm maps of the $z = 3.792$ radio galaxy, 4C 41.17 – one of the most submm-luminous HzRGs known (Chini & Krügel 1994; Dunlop et al. 1994; Ivison et al. 2000; Archibald et al. 2001; Stevens et al. 2003). We compare our data with existing 850-μm imaging and use deep *Spitzer* data as well as Very Large Array (VLA) radio imaging to locate mid-IR and radio counterparts to SMGs in the surrounding field.

Throughout, we adopt a flat cosmology, with $\Omega_{\rm m} = 0.27, \Omega_{\Lambda} = 0.73$ and $H_0 = 71\,{\rm km\,s^{-1}\,Mpc^{-1}}$ (Spergel et al. 2003).

2 OBSERVATIONS AND DATA REDUCTION

2.1 (Sub)millimetre data

A $\sim$58-arcmin^2 area, centred on 4C 41.17 and covering the entire region previously observed with SCUBA (Ivison et al. 2000), was mapped at 1200 μm using the 117-channel Max-Planck Millimeter Bolometer Array (MAMBO – Kreysa et al. 1998) on the IRAM 30-m telescope in Granada, Spain. The 30-m telescope has an effective beam of 10.7 arcsec [full width at half-maximum (FWHM)] at 1200 μm.

The data were obtained during the winter semesters of 2003–2004 and 2004–2005 in excellent weather conditions, when the atmospheric zenith opacity at 1200 μm was below 0.25 and the sky noise was low. A total observing time of 38 h (including calibrations) was obtained for the project: 9 h in 2004 March and 29 h during the 2004–2005 winter. Standard on-the-fly MAMBO scan maps, each 300 × 320 arcsec^2 in size, were made at regular grid positions 2 arcmin apart, thus ensuring uniform coverage across the entire region. The pointing and focus were checked after each map, that is, every hour or so.

The data were reduced in a standard manner using the MOPSIC software package (Zylka 1998). This involved flagging noisy bolometers, de-spiking and flat-fielding, as well as removing correlated sky noise from the time-streams of data. Finally, maps were created on a grid of 4 arcsec^2 pixel. The final signal-to-noise ratio (S/N) map is shown in Fig. 1(a).

As part of a programme to map the most-luminous HzRGs at 350 μm (Greve et al., in preparation), 4C 41.17 was observed using the Submillimeter High Angular Resolution Camera (SHARC-II) (Dowell et al. 2003) at the Caltech Submillimeter Observatory (CSO) on Mauna Kea in Hawaii. SHARC-II contains a fully sampled, pop-up bolometer array: 32 × 12 pixel, each with a size of 4.6 arcsec, giving a field of view of 2.5 × 0.9 arcmin^2. The FWHM beam size is 9.2 arcsec.

Data were taken in excellent weather conditions ($\tau_{225\,\rm GHz} \lesssim 0.05$) during a series of observing runs in 2005 February and May. Each scan was done in full-power mode by scanning the array in a 115 × 38-arcsec^2 Lissajous pattern centred on the central radio position. The pointing was checked on an hourly basis using strong submm sources and flux-calibration scans were taken regularly. The absolute calibration error was found to be less than 30 per cent. The flux calibration was done by mapping Uranus once or twice per night and then monitoring a number of secondary calibrators near the target sources throughout the night. The pointing model implemented at the CSO during the time of observations had known systematic trends which we have had to correct for in the data reduction. This was done by carefully tracking the residuals between the model and observed pointing sources as a function of elevation and zenith angle. Using these residuals, the pointing was appropriately updated for each science scan. After doing so, the typical rms pointing error was of the order of 1.5–2.5 arcsec. The data were reduced using the software CRUSH (Comprehensive Reduction Utility for SHARC-II – Kovács 2006), with the DEEP option ensuring an appropriately

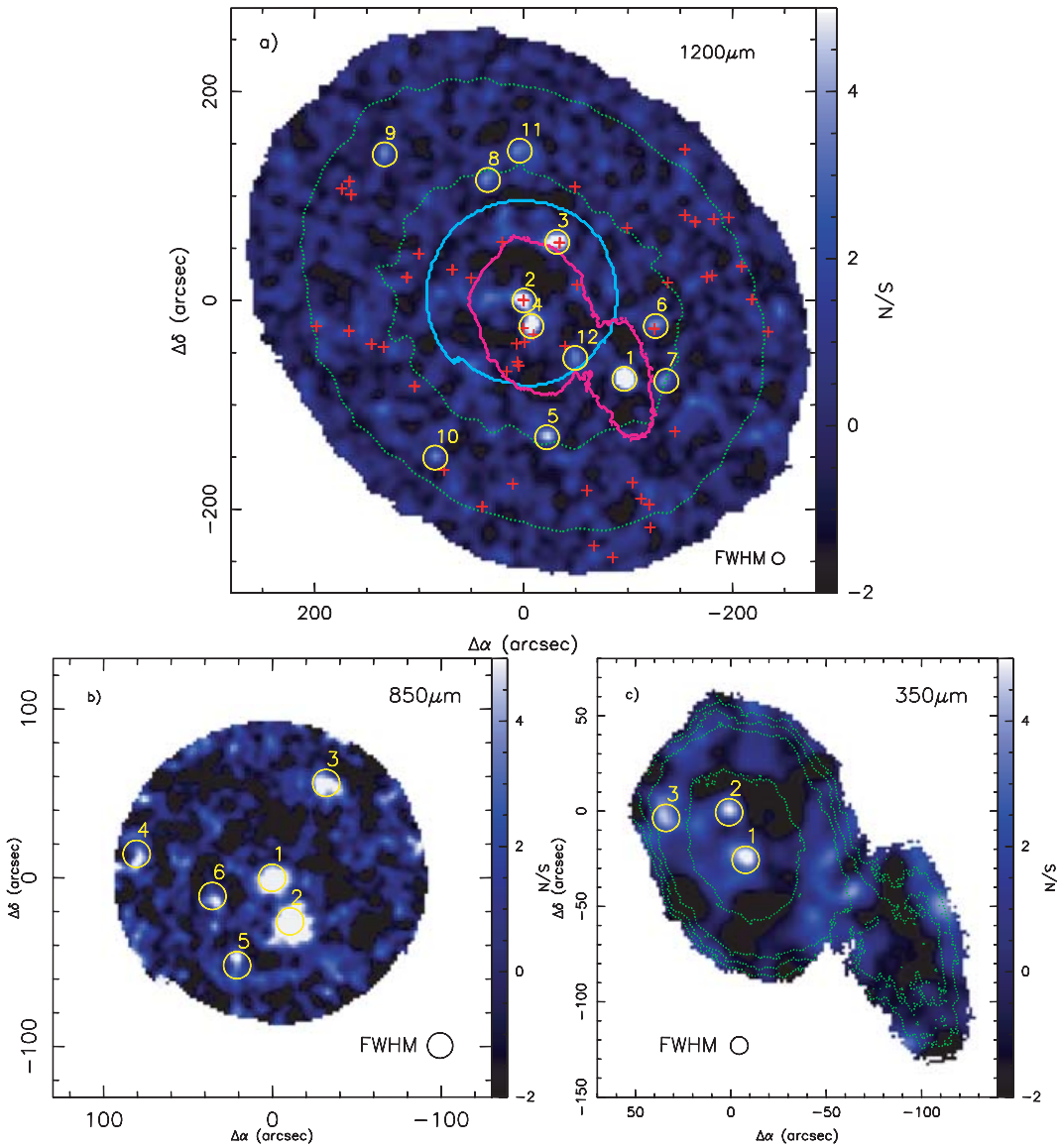

Figure 1. (a) 1200-μm MAMBO S/N map centred on 4C 41.17. The green dashed contours mark the 0.5 and 1.0 mJy beam^{-1} rms noise levels across the map. The light blue and magenta curves indicate the extend of the 850-μm SCUBA and 350-μm SHARC-II maps, respectively (Ivison et al. 2000; this work). The red crosses indicate the X-ray sources detected by *Chandra* (Smail et al. 2003b). (b) 850-μm SCUBA S/N map of 4C 41.17 (Ivison et al. 2000). (c) 350-μm SHARC-II S/N map of 4C 41.17. The 40 and 60, 70 and 80 mJy beam^{-1} rms noise levels are shown as the green dashed contours. In all three panels, we circle sources detected at a significance $\geqslant 3.5\sigma$ in yellow; numbering ranks them according to S/N (with 1 corresponding the highest ratio). Also, the axes denote the offset (in arcseconds) from the map centre RA 06:50:52.2, Dec. +41:30:30.9 (J2000). The angular resolution of the MAMBO, SCUBA and SHARC-II maps are 10.7, 14.7 and 9.2 arcsec (FWHM), respectively.

aggressive noise filtering. This is the recommended option for data reduction of faint and relatively compact sources. The final map is ∼5.2 arcmin^2 in size, covering the central region observed by SCUBA (Ivison et al. 2000) with an rms noise of ∼12 mJy beam^{-1}. The resulting 350-μm S/N map of 4C 41.17 is shown in Fig. 1(c).

Finally, we also include in the analysis of this paper the previously published 850-μm SCUBA map of 4C 41.17 (Ivison et al. 2000; Stevens et al. 2003). Details of the observations and data reduction are given in Ivison et al. (2000). Briefly, the map covers a region ∼2.5 arcmin in diameter, centred on 4C 41.17. The resolution is ∼14 arcsec (FWHM). The 850-μm S/N map is shown in Fig. 1(b).

2.2 Radio observations

Radio data were obtained using the National Radio Astronomy Observatory's (NRAO[1]) VLA in its A configuration during a period in 2003 July when a correlator fault had ruled out the intended programme of spectral line observations (Ivison et al. 2007). A small target field was required to minimize the impact of bandwidth smearing (due to the use of continuum mode), so we observed 4C 41.17 at 1400 MHz for a total of 22.2 ks over 3 d, recording two

[1] NRAO is operated by Associated Universities, Inc., under a cooperative agreement with the National Science Foundation.

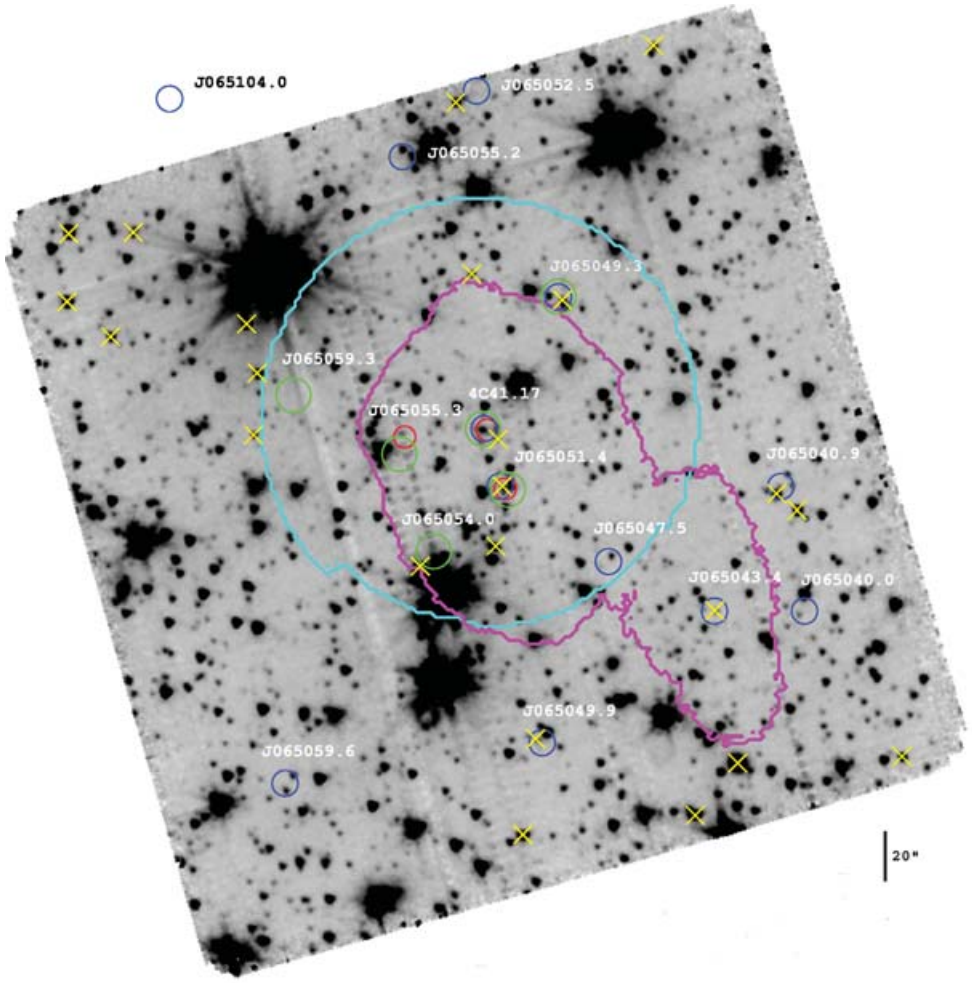

Figure 2. 5.21 × 5.21-arcmin^2 IRAC 3.6-μm image (grey-scale) of the 4C 41.17 field. 350-, 850- and 1200-μm source catalogues are overlaid as the red, green and blue circles, respectively, and the diameter of the circles corresponds to the FWHM of the CSO (9.2 arcsec), JCMT (14.7 arcsec), and IRAM 30 m (10.7 arcsec) at those three wavelengths. Sources targeted spectroscopically with Keck/LRIS are shown as the yellow crosses. For clarity, the extent of the SCUBA and SHARC-II maps has been outlined (light blue and magenta, respectively). The north is up and the east is to the left-hand side.

contiguous intermediate-frequency pairs, each covering 50 MHz in both left-hand and right-hand circular polarizations. Calibration scans of 0646+448 and 0137+331 were interspersed. Data reduction, imaging and self-calibration followed standard recipes and the resulting noise around the central radio galaxy was 23 μJy beam^{-1} (1.3-arcsec beam, FWHM), meaning the VLA had achieved a dynamic range well in excess of 10 000 with little effort.

Further VLA observations were obtained in C configuration during 2005 August – 5.1 ks centred on the brightest MAMBO source at 4860 MHz, with additional time on 0644+392 and 0137+331 for calibration. After self-calibration, the noise level in the resulting map was 24 μJy beam^{-1}, with a 3.7-arcsec beam (FWHM).

2.3 Mid-IR observations

As part of *Spitzer* Cycle 1 IRAC instrument team guaranteed time observations, the 4C 41.17 field was imaged deeply with the IRAC and MIPS cameras. These data were previously reported in Seymour et al. (2007). The data were reduced using an IDL pipeline (see Seymour et al. 2007, for details of the observations and processing). The formal 3σ point-source sensitivities for the 3.6-, 4.5-, 5.8- and 8.0-μm IRAC data were 0.8, 1.1, 3.2 and 4.3 μJy, respectively. Fig. 2 shows the 5.21 × 5.21-arcmin^2 3.6-μm image centred on 4C 41.17. Of the MIPS data, the 160-μm images were too noisy to be of any use, and only the 70- and 24-μm data were used. The 3σ point-source sensitivity of the 70- and 24-μm maps was about 1850 and 30 μJy in the deepest parts of the maps.

2.4 Near-IR imaging and optical spectroscopy

For near-IR imaging of 4C 41.17, we used z-band observations obtained during a spectroscopy run with the DEep Imaging Multi-Object Spectrograph (DEIMOS – Faber et al. 2003) on Keck on UT 2005 November 5, which was forced into imaging mode due to a fault in the motor which sets the angle of the grating. The total exposure time is 35 min, obtained as seven dithered five-minute exposures.

Optical spectroscopy of the mid-IR and radio counterparts (Section 3.2) to the SMGs detected in the 4C 41.17 field was obtained with LRIS (Oke et al. 1995) on the Keck Telescope during a run in 2006 January. Remaining space on the LRIS slit masks was used to target 24-μm emitters with IRAC counterparts. All spectroscopically targeted objects are marked by the yellow crosses in Fig. 2.

Table 1. 1200-μm MAMBO sources extracted from the 4C 41.17 field at a significance $\geqslant 3.5\sigma$.

ID	RA (J2000) ($^{\rm h}$ $^{\rm m}$ $^{\rm s}$)	Dec. (J2000) ($^\circ$ $'$ $''$)	$I^a_{1200\,\mu{\rm m}}$ (mJy beam^{-1})	$S^b_{1200\,\mu{\rm m}}$ (mJy)
MM J065043.4 + 412914[(1)]	06:50:43.4	+41:29:13.8	5.1 ± 0.4	7.5 ± 0.6
MM J065052.1 + 413031[(2)]	06:50:52.1	+41:30:30.8	2.8 ± 0.4	4.4 ± 0.4
MM J065049.3 + 413127[(3)]	06:50:49.3	+41:31:26.9	2.8 ± 0.4	4.6 ± 0.4
MM J065051.5 + 413006[(4)]	06:50:51.5	+41:30:06.4	2.3 ± 0.3	3.8 ± 0.4
MM J065049.9 + 412818[(5)]	06:50:49.9	+41:28:17.8	2.3 ± 0.5	3.0 ± 0.5
MM J065040.9 + 413006[(6)]	06:50:40.9	+41:30:06.4	1.9 ± 0.5	3.0 ± 0.6
MM J065040.0 + 412914[(7)]	06:50:40.0	+41:29:14.0	1.9 ± 0.5	3.4 ± 0.6
MM J065055.2 + 413226[(8)]	06:50:55.2	+41:32:26.3	1.7 ± 0.5	2.6 ± 0.6
MM J065104.0 + 413251[(9)]	06:51:04.0	+41:32:50.8	2.6 ± 0.7	4.3 ± 0.5
MM J065059.6 + 412800[(10)]	06:50:59.6	+41:28:00.4	2.7 ± 0.7	3.5 ± 0.6
MM J065052.5 + 413254[(11)]	06:50:52.5	+41:32:54.0	1.9 ± 0.5	3.2 ± 0.5
MM J065047.5 + 412935[(12)]	06:50:47.5	+41:29:35.0	1.3 ± 0.4	2.7 ± 0.5

[a]Peak fluxes. [b]Total flux within a $D = 15$ arcsec aperture.
[(1)]J065043.4; [(2)]4C 41.17; [(3)]HzRG850.2/J065049.3; [(4)]HzRG850.1/J065051.4; [(5)]J065049.9; [(6)]J065040.9; [(7)]J065040.0; [(8)]J065055.2; [(9)]J065104.0; [(10)]J065059.6; [(11)]J065052.5; [(12)]J065047.5.

Table 2. 350-μm SHARC-II sources extracted from the 4C 41.17 field at a significance $\geqslant 3.5\sigma$.

ID	RA (J2000) ($^{\rm h}$ $^{\rm m}$ $^{\rm s}$)	Dec. (J2000) ($^\circ$ $'$ $''$)	$I^a_{350\,\mu{\rm m}}$ (mJy beam^{-1})	$S^b_{350\,\mu{\rm m}}$ (mJy)
SMM J65051.3 + 413005[(1)]	06:50:51.3	+41:30:05.3	32 ± 6	42 ± 2
SMM J65052.1 + 413030[(2)]	06:50:52.1	+41:30:30.3	32 ± 2	40 ± 2
SMM J65055.3 + 413027[(3)]	06:50:55.3	+41:30:27.3	43 ± 2	47 ± 2

[a]Peak fluxes. [b]Total flux within a $D = 15$ arcsec aperture.
[(1)]HzRG850.1/J065051.4; [(2)]4C 41.17; [(3)]HzRG850.5/J065055.3.

The 6800-Å (D680) dichroic was used to split the light between the red and blue arm of LRIS. The 400 line mm^{-1} (B400) grism was used in the blue arm, giving a typical spectral resolution of ∼1.1 Å. For the red arm, we used the 600 line mm^{-1} (R600) grating, resulting in a spectral resolution of ∼1.3 Å. A slit width of 1.2 arcsec was adopted. The total integration time was 1 h, split into 20-min exposures, obtained during dark conditions in ∼1.1-arcsec seeing. The data were reduced using the BOGUS2006[2] IRAF package which was specially designed for reducing LRIS slitmasks.

3 RESULTS

3.1 (Sub)millimetre sources

Employing a noise-weighted convolution technique (see Greve et al. 2004b, for details), a total of 12 sources were extracted at a significance $\geqslant 3.5\sigma$ from the 1200-μm MAMBO map. The 1200-μm source catalogue is listed in Table 1, and the extracted sources are indicated in Fig. 1 as the yellow circles. Peak fluxes as well as aperture fluxes are listed in Table 1. Flux densities were determined using apertures 15 arcsec in diameter, consistent with the aperture size used by Ivison et al. (2000) to obtain total 850-μm flux densities. The same source extraction technique was applied to the SHARC-II images, resulting in three sources detected at $\geqslant 4.0\sigma$ significance. The 350-μm source catalogue is listed in Table 2. Lowering the detection threshold to 3.5σ did not result in additional detections. We list both peak and 15-arcsec aperture fluxes in Table 2.

With the 1200- and 350-μm data presented here, and the 850-μm data of Ivison et al. (2000) at our disposal, we are in a unique position to confirm or reject many of the 850-μm sources apparently associated with 4C 41.17 as first reported by Ivison et al. (2000). To this end, we make use of Fig. 2, where we have overlaid the 350-, 850- and 1200-μm source catalogues on the IRAC 3.6-μm image. Clearly, the three brightest sources detected by Ivison et al. (2000) at 850 μm (4C 41.17, HzRG850.1 and HzRG850.2[3]) are all detected at 1200 μm at a significance $\geqslant 5\sigma$ (Table 1). Out of the further three submm sources (HzRG850.3, HzRG850.4 and HzRG850.5[4]) reported by Ivison et al. (2000), one (J065059.3) coincides with a 2σ peak in the MAMBO map while the remaining two elude detection at the $\geqslant 1\sigma$ level. At face value, the lack of 1200-μm detections for two latter sources argues that they are spurious. However, due to their very low 850-μm flux densities ($S_{850} \simeq 2.4$– 2.8 mJy – Ivison et al. 2000), we would not expect to detect them at our rms noise level (∼0.5– 0.7 mJy beam^{-1}) for values of the Raleigh–Jeans slope of $\beta = 1$– 3. In summary, out of the five 850-μm sources reported by Ivison et al. (2000), excluding 4C 41.17 itself, we have confirmed the reality of the two brightest sources with our 1200-μm map but can neither confirm nor rule out the reality of the remaining three. Our unbiased recovery rate of SCUBA sources by MAMBO is therefore 40 per cent, comparable to that found in blank-field surveys (Greve et al. 2004b; Ivison et al. 2005).

Turning to the 350-μm recovery rate, we see from Fig. 2 and Table 2 that 4C 41.17 and J065051.4 are detected at 350 μm at a significance $\sim 5\sigma$. Unfortunately, both J065049.3 and J065059.3 fall outside the SHARC-II map, making it impossible to say anything

[2] http://zwolfkinder.jpl.nasa.gov/∼stern/homepage/bogus.html

[3] From this point onwards, we will refer to HzRG850.1 and HzRG850.2 as J065051.4 and J065049.3, respectively.

[4] We refer to HzRG850.3, HzRG850.4 and HzRG850.5 as J065059.3, J065054.0 and J065055.3, respectively.

about their 350-μm properties. J065054.0, however, lies within the SHARC-II map, coinciding with a negative feature. We derive a 3σ upper limit of $S_{350\,\mu m} \leqslant 54$ mJy, which is above the 350-μm peak flux density (∼40 mJy) one derives by assuming an extreme spectral index of $\beta = 3$ and a 850-μm flux of 2.8 mJy. Thus, the lack of a 350-μm counterpart to J065054.0 cannot be taken as a convincing argument against its reality as we would not expect a detection, given the depth of the 350-μm map in this region. Interestingly, however, we find a significant ($\gtrsim 4\sigma$) 350-μm source (SMM J65055.1+413027) at a position ∼5 arcsec north of J065055.3. The high significance of this source and the fact that emission is seen in two independent maps, each made from half of the SHARC-II data, leaves little doubt about the reality of this source. Is it the 350-μm counterpart to J065055.3, or an unrelated source? The expected 1σ positional uncertainty in any given direction is given by $\theta \simeq 0.6\,\mathrm{FWHM}/(\mathrm{S/N})$ (Ivison et al. 2005, 2000), which in the case of SCUBA and SHARC-II yields $\theta \sim 2.9$ and ∼1.2 arcsec, respectively. Thus, the combined positional uncertainty is $\sqrt{(2.9 + 1.2)\,\mathrm{arcsec}^2} = 3.1$ arcsec. This is in good agreement with extensive Monte Carlo simulations by Scott et al. (2002), showing that typical positional offsets of low-S/N sources detected by SCUBA are $\gtrsim 4$ arcsec. We thus conclude that the positional offset between the two sources is not significant, and we will therefore assume that they are the one and the same SMG, namely J065055.3. As was argued above, the lack of a 1200-μm detection of this source is not a strong argument against its reality. Thus, out of the three SMGs reported by Ivison et al. (excluding 4C 41.17) within the region covered by SHARC-II, at least one, but more likely two (namely J065051.4 and J065055.3), has been detected at 350 μm.

Two sources, namely J065047.5 and J065043.4, are detected at 1200 μm but not at 350 and/or 850 μm, despite lying within one or both of the SCUBA/SHARC-II maps. Of those, the most-prominent source is J065043.4, located ∼2.1 arcmin south-west of the radio galaxy, within the region covered by SHARC-II. This source is detected at $\gtrsim 10\sigma$ at 1200 μm; with a flux density of $S_{1200\,\mu m} = 7.5 \pm 0.4$ mJy, it is the brightest MAMBO source in the entire field. Unfortunately, J065043.4 is not detected at 350 μm and only a 3σ upper limit of $S_{350\,\mu m} \leqslant 70$ mJy can be put on its 350-μm flux density, largely due to the fact that the source is located in a part of the SHARC-II map which received very little integration time (about 0.5 h). Given the brightness of this source at 1200 μm, however, we would have expected a 350-μm detection (for $\beta = 1$– 3) even at the low sensitivity available in this part of the map. In Section 5.2, we speculate that this source may be a flat spectrum radio source, where the emission at 1200 μm (but not at 350 μm) is dominated by radio synchrotron emission stemming from a buried AGN. For the other source (J065047.5), which is the faintest 1200-μm source in our sample, we put 3σ upper limits on its 350- and 850-μm peak flux densities of $S_{350\,\mu m} \leqslant 30$ mJy and $S_{850\,\mu m} \leqslant 6$ mJy, respectively.

Finally, exploring the MAMBO map outside the region covered by SCUBA and SHARC-II, we find seven sources detected at a significance $\geqslant 3.5\sigma$ (Fig. 1). We note that all of these sources are significantly fainter at 1200 μm than the sources within the SCUBA/SHARC-II maps, with the exception of J065047.5 which is the faintest source in the sample.

To summarize this section, we note that the total number of SMGs, selected at 350, 850 or 1200 μm, within the region outlined by the MAMBO 4C 41.17 map is 14 (excluding 4C 41.17 itself). Of these, seven (three) have been observed (detected) at two or more (sub)mm wavelengths. Specifically, we have confirmed three out of the five SCUBA sources (not including 4C 41.17) reported by Ivison et al. (2000). Of those, one (J065051.4) was detected at both 1200- and 350-μm; another (J065049.3) lies outside the SHARC-II map but is robustly detected at 1200 μm, while the last source is detected at 350 μm but not at 1200 μm. A further two 1200-μm sources (J065047.5 and J065043.4) were covered by SCUBA and/or SHARC-II but were not detected at 850 and/or 350 μm.

In Table 3, we list our measured (sub)mm fluxes for the seven SMGs (and 4C 41.17) with observations at more than one (sub)mm wavelengths, along with all previous (sub)mm data published in the literature to date. The latter includes independent 450- and 850-μm SCUBA observations of 4C 41.17 (Ivison et al. 2000; Archibald et al. 2001; Stevens et al. 2003), as well as at 1200 μm (Chini & Krügel 1994; this work). In general, there is a good agreement between independent flux measurements – in particular, we note the excellent agreement between the 350-μm flux densities for 4C 41.17 reported by Benford et al. (1999) and ourselves. Where possible, the listed positions are an average of two or more of the 1200-/850-/350-μm positions.

3.2 Radio/mid-IR counterparts to SMGs around 4C 41.17 and spectroscopic redshifts

Due to the link between synchrotron radio and far-IR emission in starburst galaxies (Condon 1992), and the advent of radio interferometers capable of large-field, high-resolution imaging, deep radio observations are currently the most-efficient way of identifying SMGs. The positions of two-thirds of blank-field SMGs have been pinpointed in this way (Ivison et al. 1998, 2000, 2002a; Smail et al. 1999, 2000). Lacking radio observations (or in the absence of a radio counterpart), deep near- and/or mid-IR imaging can reveal the presence of either EROs or mid-IR (24-μm) sources, all of which are sufficiently rare objects on the sky that they must be either direct counterparts to the SMGs or (as is sometimes seen) nearby, associated objects.

In this section, we seek to identify radio, near-IR and/or mid-IR counterparts to the 14 SMGs extracted from our (sub)mm maps of the 4C 41.17 field, and to this end we have excised z-band, IRAC and MIPS postage stamps centred on the average (sub)mm position for each SMG (see Section 3.1) – each 30 arcsec on a side and with 1.4- and/or 4.9-GHz radio contours overlaid. The postage stamp images are shown in Appendix A (Fig. A1), where we also give a detailed description of each source.

In cases where a radio source is present, the likelihood of it being the correct identification was calculated employing the same scheme as adopted by Ivison et al. (2007), in which a radio source is considered robust if it is peaking at $\geqslant 4\sigma$, and has an integrated flux density in excess of 3σ. We adopt these criteria for both the 1.4- and 4.9-GHz fields, and find the surface density of such robust sources to be 0.65 and 0.043 arcmin^{-2}, respectively. We then search for robust radio sources within 8 arcsec of each SMG and calculate the formal significance of each submm/radio association using the method of Downes et al. (1986). To this end, we have used the radio number counts at 1.4 and 4.9 GHz from Bondi et al. (2003) and Condon (1984). A submm/radio association is considered significant if the probability, P, of it happening by chance, corrected for the number of ways that such an association could have happened by chance, is $P \leqslant 0.05$. The significance of the mm/radio associations is listed in Table 4, along with their radio flux densities and positional offsets from the (sub)mm centroids. Our relatively shallow radio imaging covers only a small fraction of the MAMBO field due to small 5-GHz primary beam and the pernicious effect of bandwidth smearing in our 1.4-GHz continuum observations. Nevertheless, the radio ID fraction is commensurate with that found in

Table 3. Summary of observed (sub)mm fluxes for SMGs in the 4C 41.17 field which have been observed at more than one (sub)mm wavelengths. All fluxes are measured within a 15-arcsec aperture. After 4C 41.17, which is listed first, the sources are listed in order of increasing RA. The positions are the average (sub)mm positions (Section 3.1).

Source	RA (J2000)	Dec. (J2000)	$S_{350\,\mu m}$ (mJy)	$S_{450\,\mu m}$ (mJy)	$S_{800\,\mu m}$ (mJy)	$S_{850\,\mu m}$ (mJy)	$S_{1200\,\mu m}$ (mJy)	$S_{1300\,\mu m}$	$S_{3000\,\mu m}$	Reference
4C 41.17	06 50 52.1	+41 30 30.6	40 ± 2	22.5 ± 8.5	17.4 ± 3.1	12.3 ± 1.2	4.4 ± 0.4	...	0.3	[1,2,3,4,5]
	...	...	37 ± 2	35.3 ± 9.3	...	12.10 ± 0.88	...	2.5 ± 0.4	...	[6,7,3,8]
	...	...	...	$3\sigma \leqslant 56$	...	11.0 ± 1.4	...	...	...	[7,9]
J065043.4	06 50 43.4	+41 29 13.8	$3\sigma \leqslant 70$	...	...	...	7.5 ± 0.6	...	...	[1]
J065047.5	06 50 47.5	+41 29 35.0	$3\sigma \leqslant 30$	...	...	$3\sigma \leqslant 6$	2.7 ± 0.5	...	...	[1]
J065049.3	06 50 49.3	+41 31 27.1	...	...	...	8.7 ± 1.2	4.6 ± 0.4	...	...	[1,2]
	...	...	...	...	...	6.2 ± 1.9	...	...	...	[2]
J065051.4	06 50 51.4	+41 30 05.8	42 ± 2	34.1 ± 9.3	...	12.2 ± 1.2	3.8 ± 0.4	...	$3\sigma \leqslant 3.3$	[1,2,10]
	...	...	...	...	...	15.6 ± 1.8	...	...	...	[7]
J065054.0	06 50 54.0	+41 29 39.0	$3\sigma \leqslant 54$	$3\sigma \leqslant 26$	...	2.8 ± 0.8	$3\sigma \leqslant 1.5$	...	...	[1,7]
J065055.3	06 50 55.3	+41 30 23.8	47 ± 2	$3\sigma \leqslant 26$	...	2.4 ± 0.8	$3\sigma \leqslant 1.5$	...	...	[1,7]
J065059.3	06 50 59.3	+41 30 45.0	...	...	...	6.5 ± 1.6	$3\sigma \leqslant 1.5$	...	...	[1,7]

Notes. [1]: this work; [2]: Stevens et al. (2003); [3]: Archibald et al. (2001); [4]: Hughes et al. (1997); [5]: De Breuck et al. (2005); [6]: Benford et al. (1999); [7]: Ivison et al. (2000); [8]: Chini & Krügel (1994); [9]: Dunlop et al. (1994); [10]: D. Downes, private communications.

Table 4. 24-/70-μm MIPS and 1.4-/4.9-GHz radio counterparts to 4C 41.17 and the 14 SMGs found in its vicinity. The MIPS 24-μm fluxes were extracted from a 9.26-arcsec aperture using aperture corrections of 3.052 from the MIPS Data Handbook. The 24-μm–(sub)mm and radio–(sub)mm association probabilities are given in boldface in cases where the association is deemed significant ($P \leqslant 0.05$).

ID	$S_{24\,\mu m}$ (μJy)	24 μm–(sub)mm separation (arcsec)	P	$S_{70\,\mu m}$ (μJy)	$S_{1.4\,GHz}$ (μJy)	$S_{4.9\,GHz}$ (μJy)	Radio–(sub)mm separation (arcsec)	P
4C 41.17	366 ± 2	0.8	**0.002**	$3\sigma \leqslant 2870$	2.35×10^5	2.53×10^4	1.3	$\mathbf{4 \times 10^{-6}}$
J065040.0	133 ± 2	6.8	0.101	...	...	...	...	...
J065040.9	349 ± 2	4.0	**0.029**	...	...	...	...	...
MIPS-1	384 ± 2	(11.6)	(0.088)	...	...	...	...	...
J065043.4	$3\sigma \leqslant 73$	...	...	...	...	109.2 ± 31.1	0.3	$\mathbf{9 \times 10^{-5}}$
	300 ± 2	7.4	0.062	...	...	...	...	...
	163 ± 2	(8.7)	(0.095)	...	...	...	...	...
J065047.5	174 ± 2	(11.4)	(0.057)	$3\sigma \leqslant 5130$	...	...	...	...
J065049.3	276 ± 2	1.1	**0.006**	$3\sigma \leqslant 4115$	...	...	...	...
	214 ± 2	4.7	0.067	...	...	...	...	...
	214 ± 2	(10.5)	(0.095)	...	...	...	...	...
	191 ± 2	(15.0)	(>0.1)	...	...	...	...	...
J065049.9	155 ± 2	1.1	**0.012**	$3\sigma \leqslant 2115$	...	...	...	...
J065051.4	448 ± 2	1.0	**0.002**	$3\sigma \leqslant 1850$	114.5 ± 31.4	...	1.0	**0.002**
J065052.5	179 ± 2	(10.2)	(0.084)	$3\sigma \leqslant 3640$	...	...	...	...
J065054.0	604 ± 2	(9.0)	**(0.043)**	$3\sigma \leqslant 5360$	...	...	...	...
J065055.2	245 ± 2	2.9	**0.031**	$3\sigma \leqslant 4680$	...	...	...	...
	153 ± 2	3.4	0.060	...	...	...	...	...
J065055.3	393 ± 2	(14.4)	(0.098)	$3\sigma \leqslant 6155$	...	...	...	...
J065059.3	$3\sigma \leqslant 65$	...	...	$3\sigma \leqslant 6079$	...	...	...	...
J065059.6	167 ± 2	3.0	**0.048**	...	...	...	...	...
	58 ± 2	5.1	0.089	...	...	...	...	...
	266 ± 2	(14.8)	(0.079)	...	...	...	...	...
J065104.0	63 ± 2	(8.6)	(>0.1)	...	...	...	...	...
	123 ± 2	(8.9)	(0.078)	...	...	...	...	...

earlier SMG studies (Ivison et al. 2002a), with statistically significant counterparts found for two SMGs (J065043.4 and J065051.4). We are not able to determine meaningful upper limits on the radio flux densities for the remainder of the SMGs, so only the robust detections are listed in Table 4.

It is seen from the last column in Fig. A1 in Appendix A that at least nine out of the 14 SMGs (not including 4C 41.17) have an 24-μm source within an 8 arcsec search radius. The same strategy used to calculate the significance of the mm/radio associations was adopted to infer the robustness of the mm/mid-IR counterparts. We used the 24-μm number counts by Papovich et al. (2004) to estimate the surface density of sources at various flux density levels. The significance of the mm/mid-IR associations is listed in Table 4, along with their mid-IR fluxes and offsets. Given the slightly larger 24-μm beam size (FWHM $\simeq$ 3.5 arcsec, compared to the $\sim$1 arcsec resolution in the radio), we also list all 24-μm sources within 15 arcsec. We

Table 5. IRAC fluxes of the MIPS and radio counterparts given in Table 4. The fluxes were extracted from a 9.26-arcsec aperture using aperture corrections of 1.091(3.6 μm), 1.117(4.5 μm), 1.100(5.8 μm) and 1.165(8.0 μm) from Lacy et al. (2005).

ID	$S_{3.6\ \mu m}$	$S_{4.5\ \mu m}$	$S_{5.8\ \mu m}$	$S_{8.0\ \mu m}$
	(μJy)	(μJy)	(μJy)	(μJy)
4C 41.17	22.9 ± 2.4	28.7 ± 3.0	38.7 ± 3.9	43.6 ± 4.4
J065040.0	118.3 ± 11.9	89.5 ± 9.0	67.2 ± 6.8	43.4 ± 4.4
J065040.9	48.5 ± 4.9	59.2 ± 6.0	57.2 ± 5.8	67.5 ± 6.8
MIPS-1	68.3 ± 6.9	57.2 ± 5.8	60.7 ± 6.1	53.2 ± 5.3
J065043.4	5.3 ± 0.6	10.4 ± 1.1	22.3 ± 2.3	17.6 ± 1.8
	18.1 ± 1.9	23.4 ± 2.4	30.1 ± 3.1	14.0 ± 1.4
	16.9 ± 1.8	18.4 ± 1.9	23.0 ± 2.3	11.2 ± 1.2
J065047.5	38.5 ± 3.9	36.1 ± 3.7	34.1 ± 3.5	25.2 ± 2.6
J065049.3	39.5 ± 4.0	42.6 ± 4.4	36.2 ± 3.7	47.2 ± 4.8
	21.7 ± 2.3	29.4 ± 3.0	30.8 ± 3.1	26.4 ± 2.7
	12.2 ± 1.3	16.3 ± 1.7	20.8 ± 2.1	19.3 ± 2.0
	10.1 ± 1.1	12.0 ± 1.3	18.5 ± 1.9	13.7 ± 1.4
J065049.9	8.8 ± 1.0	12.4 ± 1.3	14.6 ± 1.5	26.0 ± 2.6
J065051.4	15.7 ± 1.7	19.5 ± 2.0	28.5 ± 2.9	58.7 ± 5.9
J065052.5	42.6 ± 4.3	56.0 ± 5.7	47.1 ± 4.8	43.7 ± 4.4
J065054.0	170.4 ± 17.1	158.7 ± 16.0	146.8 ± 14.7	213.2 ± 21.4
J065055.2	36.9 ± 3.8	44.1 ± 4.5	47.5 ± 4.8	36.0 ± 4.6
	21.7 ± 2.3	28.7 ± 3.0	29.9 ± 3.0	21.9 ± 2.2
J065055.3	55.2 ± 5.6	45.0 ± 4.6	38.8 ± 3.9	38.1 ± 3.8
J065059.3	$3\sigma \leqslant 1.0$	1.8 ± 1.0	9.9 ± 1.0	13.9 ± 6.5
J065059.6	11.7 ± 1.3	17.7 ± 1.9	25.3 ± 2.6	22.9 ± 2.3
	15.5 ± 1.6	11.4 ± 1.2	8.2 ± 0.9	4.9 ± 0.6
	49.5 ± 5.0	59.3 ± 6.0	64.6 ± 6.5	78.5 ± 7.9
J065104.0	...	5.8 ± 2.0	...	$\leqslant 10.1$
	...	6.6 ± 2.0	...	13.9 ± 7.3

find that seven of the SMGs have statistically robust 24-μm counterparts within 8 arcsec of the (sub)mm centroid. One of these, namely J065051.4, was also identified in the radio. In the case of J065054.0, the 24-μm counterpart lies just outside the 8 arcsec search radius, yet we find it unlikely to be a random association. We find two instances, namely J065049.3 and J065055.2, where the 24-μm emission is the result of two or more sources blending together, thus complicating the identification process. In both cases, however, the bulk of the 24-μm emission can be traced to a single IRAC source, making this the most likely counterpart. This is consistent with the findings by Pope et al. (2006) that in most cases where multiple 24-μm sources are found within a SCUBA beam, only one – namely the brightest 24-μm source – is dominating the submm emission.

In total, therefore, we have robustly identified – either via their radio or via their 24-μm emission – eight out of the 14 SMGs detected. Including the 24-μm data has more than doubled the number of robust identifications, thereby illustrating the usefulness of this band for locating SMGs. Even so, due to the shallowness of our radio and mid-IR data, the combined radio and 24-μm recovery rate obtained is significantly less than the typical ∼80 per cent or so obtained for blank-field SMGs (Pope et al. 2006; Ivison et al. 2007) when extremely deep VLA and *Spitzer* data are available.

Out of the eight robustly identified SMGs, six were targeted spectroscopically, namely J065040.9, J065043.4, J065049.3, J065049.9, J065051.4 and J065054.0. From these six spectra, we could determine three robust redshifts ($0.507 \leqslant z \leqslant 2.672$), excluding them as physically associated sources to 4C 41.17. The remaining three spectra showed no evidence of any continuum nor line emission. Appendix A gives further details on the spectroscopic results.

4 ANALYSIS

4.1 Mid- and near-IR properties

With 4C 41.17 being at a redshift of $z = 3.792$, the *Spitzer* observations are sampling the near-IR/optical light coming directly from the stellar populations and/or the AGN in this system. If the near-IR emission is dominated by stellar light, we expect to see a characteristic stellar 'bump' at ∼1.6 μm (rest frame) in the combined spectral energy distribution (SED) from a composite stellar population, due to the minimum in the H^- opacity at 1.6 μm in the photospheres of cool stars (John 1988). In the case of a strong AGN contribution, however, the non-thermal emission would give rise to a power-law SED. Thus, the mere shape of the SED in this portion of the spectrum can be used as a way of discriminating between AGN-dominated systems and a significant stellar population.

The mid-IR SEDs of all eight SMGs (and 4C 41.17) identified in the radio and/or the mid-IR are shown in Fig. 3. In the case of 4C 41.17, the IRAC measurements clearly deviate from a straight power law, and instead seem to resemble a bump indicative of a stellar population. At $z = 3.792$, however, the 8.0-μm IRAC band samples the rest-frame SED at 1.7 μm, that is, just longward of 1.6 μm, thus making it hard to discern the exact shape of the stellar bump. Moreover, the 8.0-μm flux is likely to be affected by an extremely hot, AGN-heated dust component (several hundreds Kelvin hot), the presence of which is suggested by the 24-μm flux. While the lack of 16-, 70- and 160-μm detections of 4C 41.17 (Seymour et al. 2007) makes it impossible to constrain the temperature of this hot dust component, the 3σ upper limits that we are able to derive are clearly consistent with the presence of a hot dust component.

The mid-IR spectrum of J065051.4 is consistent with a power law through all of the IRAC bands, suggesting that the stellar emission is swamped by the emission from the hot, AGN-heated dust. Thus, the near- and mid-IR properties of this source indicate the presence of an AGN more strongly than in 4C 41.17, yet J065051.4 is more than two orders of magnitude less radio-luminous than 4C 41.17. There is a large spread in the observed radio-loudness of AGN, and only ∼10 per cent of them are radio-loud (e.g. Visnovsky et al. 1992; Hooper et al. 1995; Stern et al. 2000), making it more likely to find a radio-quiet AGN in the field of a radio galaxy than to find another radio-loud AGN. In fact several examples of such AGN, detected in the fields of radio galaxies, have been reported (Pentericci et al. 2000; Venemans et al. 2007).

All of the remaining seven SMGs with IRAC and/or MIPS detections (Fig. 3d) show some evidence of a stellar population. Some exhibit a clear stellar bump (J065049.9, J065043.4, J065055.2 and J065059.6), others only a hint thereof (J065049.3, J065049.9 and J065054.0). In fact J065049.9 appears to be a mixed AGN/starburst system with a mid-IR spectrum similar to that of 4C 41.17.

This picture is confirmed in Fig. 4(a) where we have plotted $S_{24\ \mu m}/S_{8.0\ \mu m}$ versus $S_{8.0\ \mu m}/S_{4.5\ \mu m}$ for 4C 41.17 and the eight SMGs with robust mid-IR counterparts. This *Spitzer* colour–colour diagram can serve as a discriminator between pure AGN-dominated systems and pure starbursts (Ivison et al. 2004, 2007), as illustrated by the clear separation between the Arp 220 (starburst) and Mrk231 (AGN) tracks in the diagram. NGC 6240, which is thought to be a 'mixed' system with significant contributions to its mid-IR/far-IR luminosity from both a starburst and an AGN, lies in the intermediate region. Clearly, J065051.4 and J065049.9 occupy the AGN region of the diagram, while the remaining seven SMGs fall within starburst region outlined by the Arp220 track. 4C 41.17 itself falls mid-way the two regions, close to the NGC 6240 track, consistent

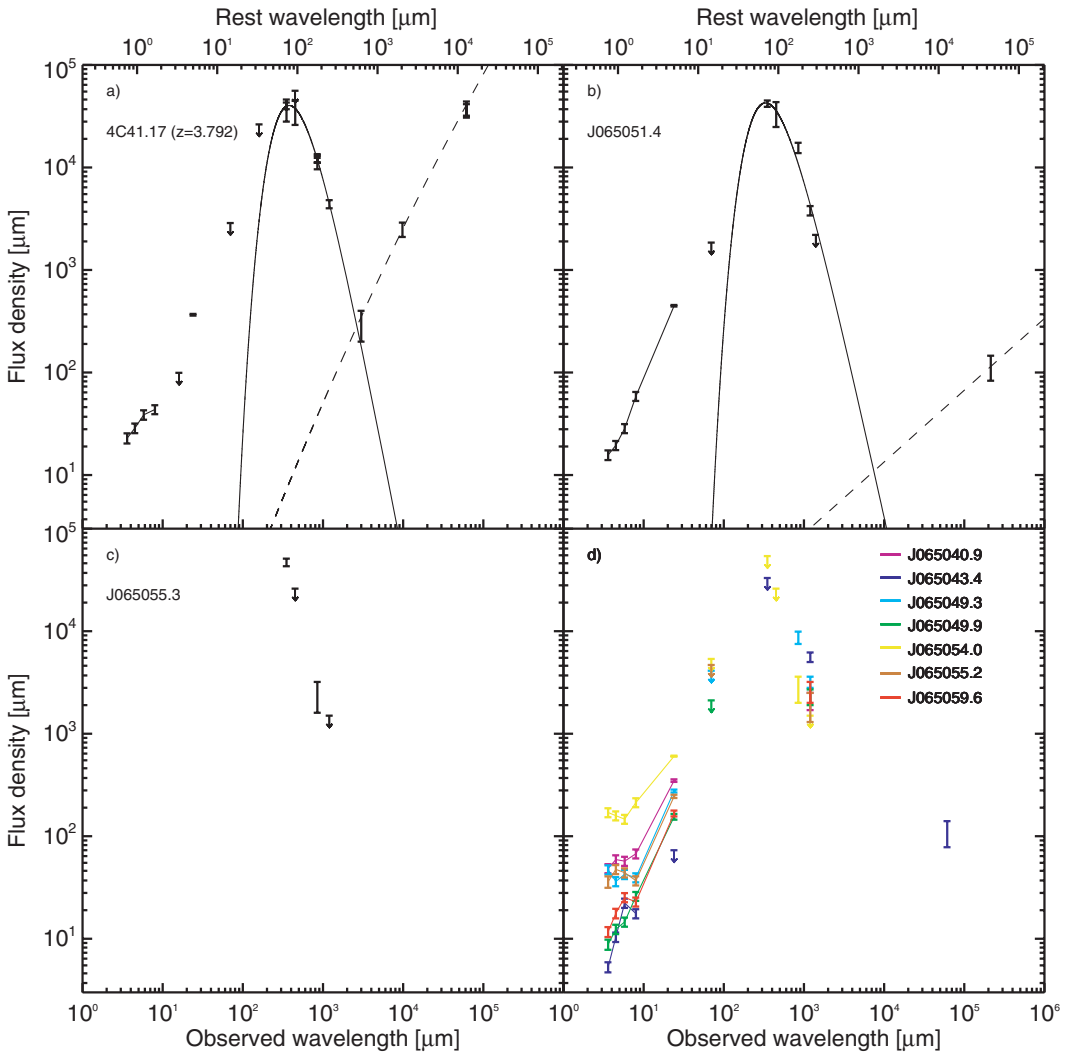

Figure 3. (a)–(c) Radio/mm/mid-IR SEDs of 4C 41.17 and the two SMGs detected at 350 μm, J065051.4 and J065055.3. Note that in the case of 4C 41.17 we have included the 16-μm upper flux limit of $3\sigma \lesssim 99$ μJy from Seymour et al. (2007). In the case of 4C 41.17 and J065051.4, grey-body laws were fitted to the far-IR/submm data while spline fits were used to model the mid-IR part of the spectra. The dust temperature ($T_{\rm d}$), spectral index (β) and an overall normalization constant were allowed to vary freely in the fitting process. The radio spectrum of 4C 41.17 was fitted with a parabola, while a power law with slope $\alpha = -0.7$ (dashed curve), consistent with the radio measurement, was adopted for J065051.4. (d) Radio/mm/mid-IR SEDs of the remaining seven SMGs with robust radio and/or 24-μm counterparts.

with its spectra showing evidence of a stellar population as well as an AGN.

Lacy et al. (2004) proposed to use the $\log S_{5.8\,\mu{\rm m}}/S_{3.6\,\mu{\rm m}}$ versus $\log S_{8.0\,\mu{\rm m}}/S_{4.5\,\mu{\rm m}}$ as a means to identify obscured AGN as well as unobscured AGN (see also Stern et al. 2005). Fig. 4(b) shows that our sources along with a sample of blank-field SMGs (Ivison et al. 2007) largely fall within the region selecting AGN. As much as four (or 50 per cent) of our sources (J065043.4, J065049.9, J065051.4 and J065059.6) are very red in both colours, and therefore likely to be AGN-dominated systems. One of these sources is J065043.4, which we show in Section 5.2 is a highly extended Lyα blob (LAB) at $z = 2.672$. Two of the sources (J065049.9 and J065051.4) with very red colours have photometric redshifts which put them at the same redshifts as 4C 41.17, while the fourth source (J065059.6) is estimated to lie at $z \sim 2.6$.

The remaining four sources, namely J065040.9, J065054.0, J065049.3 and J065055.2, are closer to the boundaries where contamination by star-forming galaxies becomes important (Stern et al. 2005). This is broadly consistent with the AGN versus starburst classification we derived from the colour–colour diagram in Fig. 4(a), where these four sources lie in the starburst part of the diagram.

Finally, we note that while half of our SMG sample have very red $S_{5.8\,\mu{\rm m}}/S_{3.6\,\mu{\rm m}}$ and $S_{8.0\,\mu{\rm m}}/S_{4.5\,\mu{\rm m}}$ colours, and therefore likely to be AGN-dominated systems, the fraction of SMGs selected from blank-field surveys with similarly red colours is much smaller (∼7 per cent). Thus, the fraction of AGN-dominated system seems to be higher in our sample than in the general SMG population. It is possible that the fact that we find two likely AGN-dominated systems (J065049.9 and J065051.4) at the same redshift as the radio galaxy is evidence for an excess of AGN in the protocluster associated with 4C 41.17 – much like what has been seen in more nearby clusters (Johnson, Best & Almaini 2003; Eckart et al. 2006).

4.2 Photometric redshifts

In addition to serving as a crude starburst versus AGN diagnostic, the 1.6-μm stellar 'bump' may also serve as a means of obtaining photometric redshifts (e.g. Sawicki 2002). Even though photometric

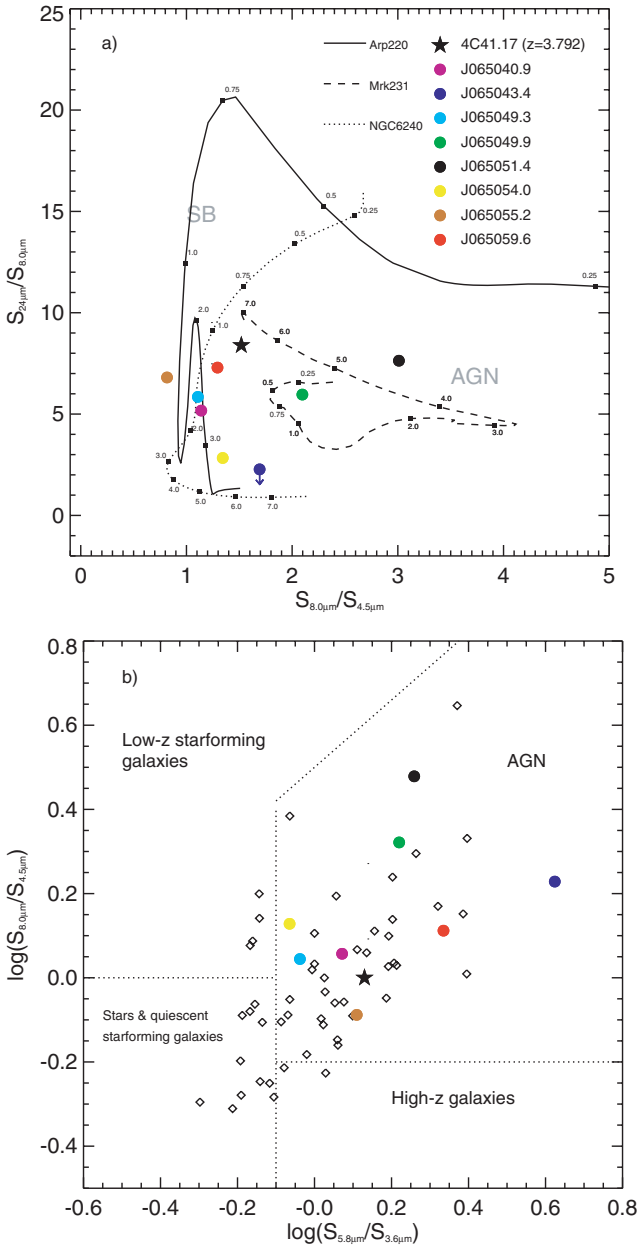

Figure 4. (a) The $S_{24\ \mu m}/S_{8.0\ \mu m}$ versus $S_{8.0\ \mu m}/S_{4.5\ \mu m}$ *Spitzer* colour–colour diagram for 4C 41.17 and the eight SMGs within the MAMBO map with robust mid-IR counterparts, identified either via the mid-IR or via the radio. The curves track the location of the local (ultra)luminous IR galaxies Arp 220 (solid curve), NGC 6240 (dotted line) and Mrk231 (dashed line) in the diagram as a function of redshift. (b) The $S_{8.0\ \mu m}/S_{4.5\ \mu m}$ versus $S_{5.8\ \mu m}/S_{3.6\ \mu m}$ *Spitzer* colour–colour diagram (Stern et al. 2005). The colour doing is the same as in (a). The diamonds represent a sample of blank-field SMGs from the SHADES survey (Ivison et al. 2007).

redshifts derived in this way are bound to be uncertain, they might be helpful for our primary purpose of establishing or refuting an overdensity of SMGs associated with 4C 41.17 by simply being able to conclude whether a source is at a redshift <4 or >4.

We therefore proceeded to derive photometric redshifts for the eight SMGs (and 4C 41.17) with robust mid-IR/radio identifications. The photometric redshifts were estimated simply by identifying the IRAC channel most likely to represent the 1.6-μm rest-frame stellar feature. The results are listed in Table 6. In addition to the eight SMGs and 4C 41.17, we also included a spectroscopically identified 24-μm source in order to see how well our photometric redshift technique recovers the true redshift (this source is located 11.6 arcsec south-west of J065040.9 and is denoted by MIPS-1 – Table 4).

Table 6. Spectroscopic and photometric redshifts.

ID	$z_{\rm phot,IRAC}$	$z_{\rm phot,radio/submm}$	$z_{\rm spec}$
4C 41.17	∼4		3.792 ± 0.001
J065040.0	...	...	...
J065040.9	∼1.8	...	...
MIPS-1	< 1.3	...	0.909 ± 0.002
J065043.4	∼2.6	> 2.8	2.672 ± 0.001
J065047.5	...	> 1.7	...
J065049.3	< 1.3	$1.2 - 16$	1.184 ± 0.002
J065049.9	∼4	...	...
J065051.4	...	$2.0 - 4.3$	...
J065052.5	...	...	...
J065054.0	< 1.3	$1.5 - 16$	0.507 ± 0.020
J065055.2	∼1.8	...	...
J065055.3	...	...	...
J065059.3	...	...	...
J065059.6	∼2.6	...	...
J065104.0	...	...	...

For the five sources (4C 41.17, J065040.9, J065043.4, J065055.2 and J065059.6) which exhibit a relatively well-defined stellar 'bump', we are able to infer a single value for the photometric redshifts, while only upper limits can be inferred for the remaining three sources (J065049.3, J065054.0 and MIPS-1) where the stellar bump appears to have been redshifted into the 3.6-μm channel or bluewards of it. The upper limits derived in those three latter cases assume that the 1.6-μm (rest-frame) stellar feature falls in or below the 3.6-μm (observed frame) channel. Only two out of the five sources with spectroscopic redshifts have well-defined stellar bumps, but in both the cases (4C 41.17 and J065043.4) we find good agreement between their photometric and spectroscopic redshifts. The upper limits on the photometric redshifts for the remaining three sources (J065049.3, J065054.0 and MIPS-1) are consistent with their spectroscopic redshifts. Thus, it seems not only that redshift estimates based on the 1.6-μm feature are robust when a well-defined stellar bump is present in the mid-IR spectrum, but also that meaningful upper limits can be placed even when this feature is absent (and the spectrum is not dominated by an AGN). The photometric redshifts for J065040.9, J065055.2 and J065059.6 are ∼1.8, ∼ 1.8 and ∼2.6, respectively, but unfortunately we do not have spectroscopic redshifts for any of those three sources.

In a further attempt to get a handle on the redshifts of our SMG sample, we have looked at their radio/submm/mm colours as photometric redshift indicators. Historically, the first photometric redshift indicator considered for SMGs was the 850-μm/1.4-GHz spectral index (Hughes et al. 1998; Carilli & Yun 1999), which makes use of the steep opposite slopes of the radio and (sub)mm parts of a typical starburst SED. The radio-submm spectral index, however, is only useful as a redshift indicator at redshifts $\lesssim$3, due partly to the rapid drop-off in the detectability of SMGs at higher redshifts in even the deepest radio maps. Of the (sub)mm colours one may use the 850-/1200-μm flux ratio, for example, which is expected to be a strong function of redshift beyond $z \gtrsim 3$ (Eales et al. 2003; Greve et al. 2004b), while the 350-/850-μm and 350-/1200-μm flux ratios are mostly sensitive to the redshift range $1 \lesssim z \lesssim 3$. In Fig. 5, we

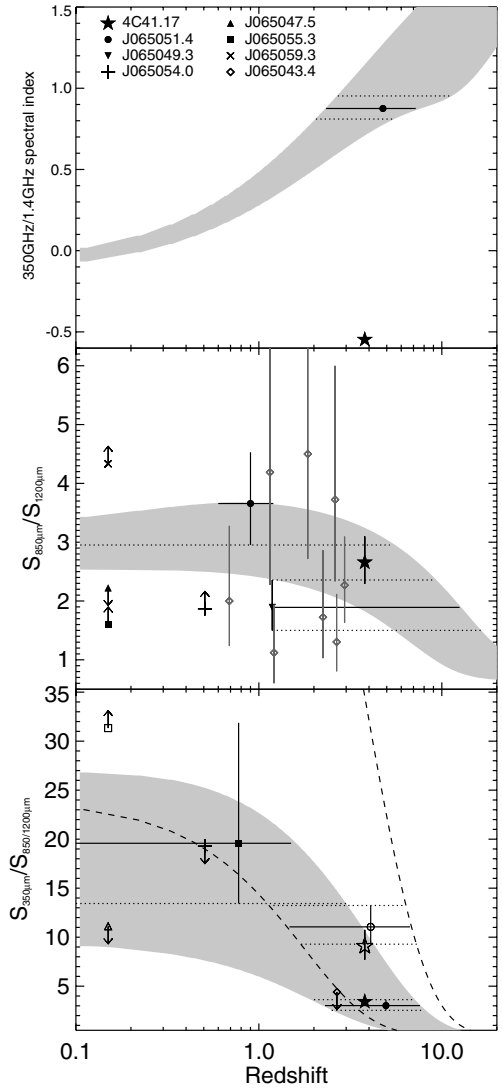

Figure 5. Top panel: the 1.4 GHz to 350 GHz spectral indices for 4C 41.17 and J05651.4. Middle panel: the 850-/1200-μm flux ratio for 4C 41.17 and the six SMGs in our sample detected with SCUBA and/or MAMBO (Table 3). Also shown are the flux ratios for a sample of robust blank-field SMGs identified from SCUBA and MAMBO surveys of the Lockman Hole East (Greve et al. 2004b; Ivison et al. 2005). Bottom panel: the 350-/850-μm (filled symbols) and 350-/1200-μm (open symbols) for the SMGs in our sample which have been observed at 350 μm and 850 or 1200 μm. In the two top panels, the grey-shaded region outlines the range of flux ratios allowed by modified blackbody SEDs with $T_{\rm d} = 20$– 70 K and $\beta = 1.0$– 2.0. In the lower panel, the grey-shaded region and the region outlined by the dashed curves mark the range of 350-/850-μm flux and 350-/1200-μm flux ratios, respectively, as a function of redshift allowed by these models. Where possible, the sources have been placed at their spectroscopic redshifts. Otherwise, sources were placed at the centre of the photometric redshift range suggested by their flux ratio, or, in the case where only upper/lower limits were available, placed at $z = 0.15$. For sources with well-determined flux ratios, the horizontal dotted lines have been drawn to outline the range of possible redshifts allowed by the SED models within the errors of the flux ratios.

compare the above flux ratios as derived for our sample with the predicted flux ratios (as a function of redshift) for a broad range of possible grey-body far-IR/submm SEDs ($T_{\rm d} = 35$– 65 K and $\beta = 1.0$– 2.0), and use these model predictions to constrain the possible redshift range for our sources.

As expected given that 4C 41.17 is a radio-loud AGN, its 850-μm-to-radio spectral index [$\alpha = 0.42 \log (S_{1.4\,\rm GHz}/S_{350\,\rm GHz})$] lies below the model predictions by more than an order of magnitude. Its (sub)mm flux ratios, on the other hand, are consistent with the SED models at $z \simeq 3.8$.

The radio-to-submm index of J065051.4 places it at a redshift of $2.1 \lesssim z \lesssim 7.2$. The 850-/1200-μm flux ratio of J065051.4 is at the high end of what is typically observed in blank-field SMGs but consistent with the models, given the large error bars. We put an upper limit on the redshift of this source of $z \lesssim 5.2$. The low 350-/850-μm and 350-/1200-μm flux ratios of this source yield possible redshift ranges of $2.0 \lesssim z \lesssim 7.7$ and $1.2 \lesssim z \lesssim 4.3$, respectively. Thus, the four flux ratios for J065051.4 yield consistent photometric redshift ranges, and assuming that the true redshift should be found in the overlap region of these four redshift ranges, we constrain the likely redshift range for this source to $2.0 \lesssim z \lesssim 4.3$.

The 850-/1200-μm flux ratio for J065049.3 is on the low side, barely consistent within the errors, of the expected range of flux ratios predicted by the model and thus, in the absence of a spectroscopic redshift, would favour a redshift range of $1.2 \gtrsim z \gtrsim 16$, where the uncertainties in the flux ratio have been taken into account. The low end of this redshift range is consistent with the spectroscopic redshift ($z = 1.184$), and suggest that we have correctly identified the mid-IR counterpart to this SMG and thus its redshift. This scenario is further strengthened by the X-ray and z-band detections of the favoured 24-μm candidate counterpart. Also, we note that the flux ratio is well within the range observed for blank-field SMGs with spectroscopic redshifts in the range $0.7 \lesssim z \lesssim 3$.

For the remaining sources, only upper and/or lower limits are available for the various flux ratios, severely weakening the constraints that can be put on the redshifts of these sources. In the case of J065054.0 where the redshift is known from spectroscopy, we find that the upper limit on the 350-/850-μm flux ratio for this source is consistent with the model values at $z = 0.507$. For J065043.4 where we find a robust spectroscopic redshift of $z = 2.672$, we find a 350-/1200-μm flux ratio which is consistent (albeit marginally) with the range of flux ratios from the models. Of the three sources with no spectroscopic redshifts, we find that J065047.5 has consistent 350-/1200-μm and 850-/1200-μm flux ratios which both point towards high redshifts ($z \gtrsim 1.7$).

4.3 Far-IR luminosities, dust temperatures and masses

SHARC-II observations provide a particularly important datum in the SEDs of galaxies at redshifts beyond unity. At such redshifts, 350-μm observations sample very close to the rest-frame dust peak at ∼100-μm, allowing for more accurate estimates of dust temperature and far-IR luminosity than can be made with 850- and/or 1200-μm observations only. SCUBA and MAMBO observations, however, are better at constraining the Rayleigh–Jeans tail, and the combination of short- and long- (submm) wavelength observations is therefore potentially very powerful, allowing for a much better characterization of the full far-IR/submm SED.

Two of the SMGs (J065051.4 and J065055.3) presented here, and 4C 41.17 itself, were detected at 350 μm in addition to 850- and/or 1200-μm. The radio and far-IR/mm SEDs of these three sources are shown in Fig. 3 along with the remaining five SMGs with robust 24-μm/1.4-GHz identifications (see Table 3).

Only 4C 41.17 and J065051.4 have robust detections at four or more (sub)mm wavelengths, and as a result we only attempted to derive dust temperatures and spectral indices for those two sources. The SEDs were fitted with an optically thin grey-body law of the

Table 7. Derived physical properties for 4C 41.17 and the 14 SMGs in our sample. Redshifts in parentheses are photometric redshifts.

Source		$T_{\rm d}$ (K)	β	$L_{\rm FIR}$ ($\times 10^{13}\,{\rm L}_\odot$)	M_d ($\times 10^{9}\,{\rm M}_\odot$)	SFR (${\rm M}_\odot\,{\rm yr}^{-1}$)
4C 41.17	3.792	44 ± 2	1.6 ± 0.1	1.5	0.8	900
J065051.4	3.792	47 ± 2	1.6 ± 0.1	2.1	0.8	1200
J065040.0[a]	...	40.0	1.5	2.2	...	1300
J065040.9	(1.8)	...	...	0.9	1.0	500
J065043.4	2.672	...	...	2.3	2.5	1300
J065047.5[a]	...	...	...	1.7	...	1000
J065049.3	1.184	...	...	0.6	0.7	400
J065049.9	(4)	...	...	0.9	1.0	500
J065052.5[a]	...	...	...	2.0	...	1200
J065054.0	0.507	...	...	0.1	0.1	100
J065055.2	(1.8)	...	...	0.8	0.9	500
J065055.3[a]	...	...	...	0.5	...	300
J065059.3[a]	...	...	...	1.2	...	700
J065059.6	(2.6)	...	...	1.1	1.2	600
J065104.0[a]	...	...	...	2.7	...	1600

[a]The far-IR luminosity was calculated using $L_{\rm FIR}/{\rm L}_\odot = 1.9 \times 10^{12}\,(S_{850\,\mu{\rm m}}/{\rm mJy})$, see Section 4.3 for details.

form: $S_{\nu_{\rm o}} \propto \nu_{\rm r}^{\beta} B(\nu_{\rm r}, T_{\rm d})$, where $S_{\nu_{\rm o}}$ is the flux at the observed frequency $\nu_{\rm o}$, β is the grain emissivity, $T_{\rm d}$ is the dust temperature, and $B(\nu, T_{\rm d})$ is the Planck function. All the far-IR/submm data listed in Table 3 for these two sources, except for upper limits, were used in the fit. All three parameters involved in the fit, namely $T_{\rm d}$, β and an overall normalization factor, were allowed to vary freely. Also, given the high likelihood that J065051.4 is at the same redshift as 4C 41.17 (Section 5.1), we adopted a redshift of $z = 3.792$ when fitting the SED of this source. The resulting grey-body fits are shown as the solid curves in Figs 3(a) and (b). The corresponding physical quantities, including the far-IR luminosity, dust masses and star formation rate, are listed in Table 7.

We also include the radio data in Fig. 3 in order to compare with the far-IR/submm part of the SED, and in particular to check whether the synchrotron radiation contributes significantly to the thermal dust emission in any of the sources. For 4C 41.17 radio data were compiled from the WENSS (325 MHz; Rengelink et al. 1997), Texas (365 MHz; Douglas et al. 1996), Green Bank Northern Sky Survey (1.4 GHz; White & Becker 1992) and the NRAO VLA Sky Survey (1.4 GHz; Condon et al. 1998), and fitted with a parabolic function. While the synchrotron emission can account for all of the observed 3-mm emission, its contribution to the emission at (sub)mm wavelengths is negligible ($\lesssim 1$ per cent of the measured 1200- or 850-μm flux densities). Thus, as expected, the (sub)mm emission originating from 4C 41.17 is dominated by thermal emission from dust (Dunlop et al. 1994). The same goes for J065051.4, if we assume a radio spectrum normalized to the 1.4-GHz flux and with a slope of $\alpha = -0.7$ (where $S_\nu \propto \nu^\alpha$).

For the sources for which spectroscopic or reliable photometric redshifts were available, far-IR luminosities were derived by integrating their SEDs over the wavelength range $\lambda = 40$– 1000 μm. While we were able to integrate over the best-fitting SED in the case of 4C 41.17 and J065051.4, for the remaining seven sources with redshift estimates we simply adopted a grey-body SED (with $T_{\rm d} = 40$ K and $\beta = 1.5$), normalized to its 850-μm flux. When no 850-μm flux was available, we used 1200-μm flux densities (or if that was not available, the 350-μm flux density) together with the scaling relation, $S_\nu \propto \nu^{2+\beta}$ to derive $S_{850\,\mu{\rm m}}$. Far-IR luminosities for the last six sources with no robust redshift estimate were derived using $L_{\rm FIR}/{\rm L}_\odot = 1.9 \times 10^{12}\,(S_{850\,\mu{\rm m}}/{\rm mJy})$ which is valid for a grey-body SED with $T_{\rm d} = 40$ K and $\beta = 1.5$. The above relation for the far-IR luminosity applies over the redshift range ∼2–4 with typical uncertainties of about a factor of ∼2– 3 (Blain et al. 2002); but the uncertainties could of course be even higher if the sources do not lie in this redshift range.

The dust masses giving rise to the far-IR/submm emission were estimated following the prescription by Hildebrand (1983):

$$M_{\rm d} = \frac{1}{1+z}\,\frac{S_{\nu_{\rm o}} D_{\rm L}^2}{\kappa(\nu_{\rm r}) B(\nu_{\rm r}, T_{\rm d})}, \qquad (1)$$

where $\nu_{\rm o}$ and $\nu_{\rm r}$ are the observed and rest-frame frequencies, respectively, $S_{\nu_{\rm o}}$ is the observed flux density, $D_{\rm L}$ is the luminosity distance, and $\kappa(\nu_{\rm r})$ is the mass absorption coefficient in the rest frame. For the latter we have adopted a value of $\kappa(\nu_{\rm r}) = 0.11\,(\nu_{\rm r}/352\,{\rm GHz})^\beta$ in units of ${\rm m}^2\,{\rm kg}^{-1}$. Dust masses were only derived for sources with redshift estimates. Star formation rates were estimated using $SFR/{\rm M}_\odot\,{\rm yr}^{-1} = L_{\rm FIR}/1.7 \times 10^{10}\,{\rm L}_\odot$ (Kennicutt 1998). The resulting far-IR luminosities, dust masses and star formation rates are listed in Table 7. The star formation rates should be considered as upper limits as they were derived on the basis that the far-IR luminosities of these systems are dominated by star formation, and not AGN-activity.

5 DISCUSSION

5.1 Is 4C 41.17 a highly overdense region of the Universe?

Taken at face value, the 14 SMGs (not including 4C 41.17 itself) detected within the 58-arcmin^2 region outlined by the MAMBO map correspond to a surface density of ∼0.24 arcmin^{-2} or, equivalently, 860 deg^{-2}. If we adopt a more conservative approach and only include those 11 SMGs which have either been confirmed or been detected for the first time at $\geqslant 3.5\sigma$ at 1200 μm with MAMBO, we find an average surface density of ∼675 deg^{-2}.

This is perfectly consistent with the 1200-μm blank-field number counts which yield $N(S_{1200\,\mu{\rm m}} \geqslant 2\,{\rm mJy}) \sim 700\,{\rm deg}^{-2}$ – so obtained by (mildly) extrapolating from the observed 1200-μm counts in the flux range ∼2.8– 5.3 mJy (Greve et al. 2004b). Thus, even in the most-optimistic scenario where all 14 SMGs are real, we find the surface density of SMGs, when averaged over the entire MAMBO map, to be no more than ∼20 per cent above the blank field. It is

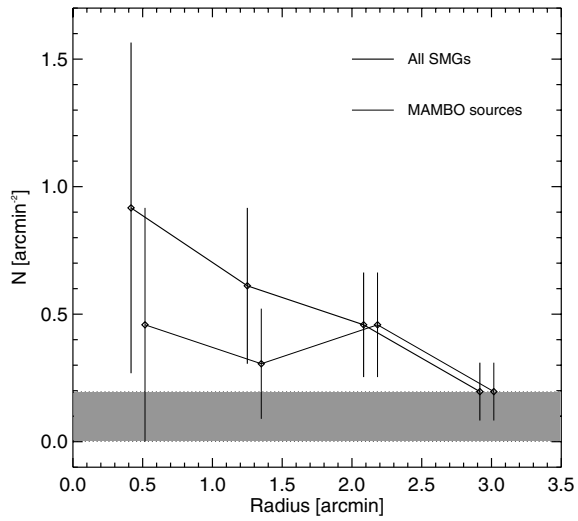

Figure 6. The average surface density of SMGs within 50-arcsec-wide annuli at 50, 100, 150 and 200 arcsec from 4C 41.17 (but not including the radio galaxy itself). The thick curve represents the surface density profile using all 14 SMGs in our sample, while the thin curve is derived using only the sources detected at 1200 μm with MAMBO. The error bars are Poisson errors. The grey-shaded region outlines the blank-field surface density of 1200-μm selected sources brighter than 2 mJy ($\sim$0.19 arcmin^{-2} – upper edge) and 10 mJy ($\sim$0.03 arcmin^{-2} – lower edge).

possible, however, that by averaging over the entire MAMBO map, which is a relatively large area, any presence of an SMG overdensity may have been 'diluted', and thus does not appear to be significant. If 4C 41.17 really is an overdense region, however, we would expect a steady increase in the source concentration towards the radio galaxy, with most of the MAMBO sources at the outskirts of the map belonging to the blank-field SMG population, while the fraction of SMGs associated with 4C 41.17 increases towards the centre.

That this may be the case is hinted at in Fig. 6 where we have plotted the surface density of sources within 50-arcsec-wide annuli centred on the radio galaxy as a function of radius from the galaxy. Although the uncertainties are substantial due to the small number of sources available, we see a tentative trend showing the SMG surface density increasing towards the centre. The surface densities in the first three inner bins using all 14 SMGs are approximately five, three and three times that of the 1200-μm blank-field source density (brighter than 2 mJy – see Fig. 6), respectively, while we find overdensities of factors of $\sim$2 using the MAMBO sources only. The existence of an SMG overdensity around 4C 41.17 can also be argued from the fact that if we assume a field surface density of $N(S_{1200\,\mu\mathrm{m}} \geqslant 2\,\mathrm{mJy}) \sim 700\,\mathrm{deg}^{-2}$, then we would expect to find the first mm source within a radius of 76 arcsec, the second within 108 arcsec, the third within 133 arcsec, etc. What we observe, however, is three sources within the inner 76 arcsec, which is thus clearly where the overdensity occurs, while no evidence for an overdensity is seen at larger radii.

If we restrict the analysis to the inner 1.5 arcmin, which roughly corresponds to the radius of the SCUBA map, and consider all five SCUBA sources within it real, we infer an overdensity only 30 per cent above that of the blank field, where we have assumed $N(S_{850\,\mu\mathrm{m}} \geqslant 2.5\,\mathrm{mJy}) \sim 2000\,\mathrm{deg}^{-2}$ for the latter (Coppin et al. 2006). Three MAMBO sources and two SHARC-II sources are found within this radius, corresponding to overdensities of approximately four and ten times, respectively, where we have used $N(S_{350\,\mu\mathrm{m}} \geqslant 40\,\mathrm{mJy}) \sim 100\,\mathrm{deg}^{2}$ from a 350-μm number count model (A. W. Blain, private communications) and $N(S_{1200\,\mu\mathrm{m}} \geqslant 2.7\,\mathrm{mJy}) \sim 380\,\mathrm{deg}^{-2}$ (Greve et al. 2004b). If we further restrict ourselves to only include J065049.3 and J065051.4, which are the two brightest SCUBA/MAMBO sources within 1.5 arcmin of the radio galaxy, we find overdensities of approximately seven and 10 times above the 850- and 1200-μm blank-field values. Thus, it is the combination of bright sources close to the radio galaxy, which makes the overdensity significant.

If the SMG overdensity depicted in Fig. 6 is correct, it seems to have a scalelength of $\sim$1 arcmin (or $\sim$430 kpc). In contrast, the SMG overdensity associated with TNJ1338−1942 was more or less evenly distributed over a much larger area (De Breuck et al. 2004). If we compare with observed overdensities of Lyα emitters towards HzRGs, we find typical scalelengths of 5–10 arcmin that is again much larger than the SMG overdensity towards 4C 41.17. The one HzRG field (PKS1138−262 at $z = 2.156$) with Hα emitters and EROs (Kurk et al. 2004) shows that these are concentrated within the central 40 arcsec. It was suggested that the Lyα emitters are younger, and not relaxed with respect to the central cluster potential yet, while EROs and Hα emitters were older. Extrapolating this to (sub)mm galaxies and especially to $z = 3.8$ is not straightforward, however.

The above line of arguments is often taken as evidence that 4C 41.17 as well as other HzRGs (De Breuck et al. 2004) are overdense regions harbouring multiple far-IR/(sub)mm luminous systems associated with the radio galaxy. Deep SCUBA maps of the central region of seven HzRGs by Stevens et al. (2003), including 4C 41.17, yield central overdensities of SMGs brighter than 5–6 mJy at 850 μm of more than a factor of 2 associated with these systems. In three cases, they found a companion source brighter than 8 mJy, corresponding to overdensities of approximately seven times that of the field. A wide 1200-μm MAMBO survey of the $z = 4.1$ radio galaxy TN J1338−1942 resulted in the detection of 10-mm sources within a 25.6-arcmin^2 field (De Breuck et al. 2004), corresponding to an overdensity approximately three times that of the blank field.

In the case of 4C 41.17, however, which is one of the richest and complex (sub)mm fields known, we have spectroscopically demonstrated that at least three of the SMGs in the field, namely J065043.4, J065049.3 and J065054.0 – of which the first two were previously thought to be part of an SMG overdensity associated with 4C 41.17 – are in fact at much lower redshifts, and therefore completely unrelated to the radio galaxy.

If we exclude J065043.4, J065049.3 and J065054.0, which we have demonstrated to lie at redshifts <3, from the analysis, we find overdensities of approximately five, two and two times that of the 1200-μm blank field in the inner three bins in Fig. 6. If we further exclude the three sources (J065040.9, J065055.2 and J065059.6) where the photometric redshifts indicate $z < 3$, we estimate overdensities of approximately five, two and one times that of the 1200-μm blank field. Thus, we find that the evidence for an overdensity of SMGs within the inner 50 and 100 arcsec remains relatively robust with the current, sparse spectroscopic data (but might disappear with more complete spectroscopy).

It should be noted that while we have been unable to obtain a spectroscopic redshift for J065051.4, we feel that the likelihood of this source not being part of the same system as 4C 41.17 is small, given its proximity to the radio galaxy and the fact that weak, extended (sub)mm emission is seen to bridge the two sources (Appendix A, Fig. A3). Furthermore, the (sub)mm photometric redshift of J065051.4 is consistent with this scenario. None the less, the fact that J065051.4 is the only source for which there is relatively

firm evidence of it belonging to 4C 41.17, and the fact that this has been shown (via spectroscopy) not to be the case for three other sources close to 4C 41.17, illustrate that caution is needed in the absence of solid spectroscopic evidence when claiming physical associations between HzRGs and observed SMG overdensities, especially when the latter are based on small-number statistics.

Based on our spectroscopic and photometric redshifts, we conclude that in the 4C 41.17 field, nearly half of the apparently associated SMGs are in fact foreground sources, that is, at $z < 3.8$. This is fully consistent with the known source density and redshift distribution of blank-field SMGs (Scott et al. 2002; Greve et al. 2004b; Chapman et al. 2005). Finally, we note that we find no spectroscopic evidence for a foreground cluster which may be gravitationally amplifying the 4C 41.17 field.

5.2 The nature of J065043.4

With a flux density of 7.5 mJy, J065043.4 is by far the brightest 1200-μm source in the 4C 41.17 field. What powers the extreme far-IR luminosity of this source? In a large 1200-μm survey of the low-density cluster, Abell 2125, Voss et al. (2006) uncovered four unusually bright background sources with flux densities similar to those of J065043.4 ($S_{1200\,\mu m} \simeq 10$– 90 mJy). Three of these sources were found to be flat-spectrum radio sources and deemed likely to be quasars based on their X-ray luminosities. These mm-bright flat-spectrum radio sources were overdense by a factor of 7–9 compared to the expected surface density, derived from the number counts of flat-spectrum radio sources and a reasonable model for their behaviour at 90–250 GHz. While J065043.4 seems quite similar to the Voss et al. quasars in terms of mm and radio brightness, we are unable to determine whether it is a flat-spectrum radio source because we lack a meaningful upper limit at 1.4 GHz (see Section 3.2). Arguing against J065043.4 being a flat-spectrum source, such galaxies tend to be type 1 AGN – bright optically, and in X-rays – quite unlike J065043.4. Further observations are needed to determine the radio properties of J065043.4.

The optical spectrum of J065043.4 shows only one very strong emission line which we identify as Lyα at $z = 2.672$. In a 2D rendition of the spectrum (Appendix A, Fig. A2a), the Lyα emission is spatially extended out to 13.5 arcsec (∼110 kpc) and there is evidence of a velocity shear across the line, which could be due to either rotation or infall/outflow.

Extended Lyα haloes have been observed around a variety of objects at high redshifts, including HzRGs (e.g. Reuland et al. 2003) and SMGs (Ivison et al. 1998; Chapman et al. 2004). Deep narrow-band imaging surveys specifically designed to select such 'LABs' have been undertaken (e.g. Fynbo, Møller & Warren 1999; Steidel et al. 2000). Nevertheless, LABs such as J065043.4, with Lyα emission extending beyond 50 kpc, are very rare; only a dozen or so have been found. It is unclear what powers these very extended LABs. Plausible explanations are a large-scale superwind stemming from a massive, dust-enshrouded starburst (Taniguchi & Shioya 2000; Ohyama et al. 2003), a buried QSO (Haiman & Rees 2001; Weidinger et al. 2005), or simply cooling radiation from infalling gas within a dark matter halo (e.g. Haiman, Spaans & Quataert 2000).

J065043.4 is undetected at 24 μm – unusual but not unique for an SMG; its single emission line, Lyα, is perfectly normal (Chapman et al. 2005). It is the third known submm-bright LAB and all three have different properties – typical of this intriguing, heterogeneous population (e.g. Ivison et al. 2000). A more detailed study of J065043.4 is in progress (Greve et al., in preparation).

6 SUMMARY

We have conducted wide-field imaging at (sub)mm, mid-IR and radio wavelengths of the luminous, $z = 3.792$ radio galaxy, 4C 41.17. In addition to the radio galaxy itself, we robustly confirm two bright sources previously detected by SCUBA in its immediate vicinity. Out of another three very faint sources detected by SCUBA, we tentatively confirm one at 350 μm. Further nine sources are detected (at the 3.5σ level) at 1200 μm in this field. Thus, a total of 14 (sub)mm galaxies are found within a ∼4.2 arcmin radius of 4C 41.17.

Using our radio and 24-μm data, we find statistically significant counterparts to 8/14 (57 per cent) of our SMGs. We targeted six of these robust counterparts spectroscopically using LRIS on Keck, and were able to infer reliable spectroscopic redshifts in four cases. All four were found to lie at redshifts well below that of the radio galaxy, thus ruling out any physical association with 4C 41.17. Comparing the spectroscopic redshifts with redshifts derived from the 1.6-μm stellar feature suggests that the latter is a reliable photometric redshift indicator. Out of the four SMGs with no spectroscopic redshifts, we use the 1.6-μm stellar bump to estimate their redshifts and find only one to be consistent (within the errors) with the redshift of 4C 41.17.

Armed with our spectroscopic redshifts, we find that nearly half of the SMGs apparently associated with 4C 41.17 are in fact foreground sources. We have constrained the overdensity of SMGs within a 50-arcsec^2 region of 4C 41.17 to be approximately five times that of the typical surface density observed in blank fields. This drops off as a function of distance from the radio galaxy, with an apparent scalelength of ∼1 arcmin.

Deeper, wider (sub)mm surveys of of HzRGs are needed to improve the statistics on source overdensities and to probe the filamentary structures expected to be channelling material into these regions. These surveys should be complemented by high-resolution (sub)mm interferometry and deep radio imaging to pinpoint positions to determine source morphologies. Finally, deep spectroscopy is required to test for membership of a HzRG-related protocluster, although the imminent arrival of broad-band heterodyne receivers suggests that CO spectroscopy may prove to be a more efficient way of determining redshifts for these SMGs.

ACKNOWLEDGMENTS

We are grateful to Darren Dowell and Colin Borys for helpful discussion relating to SHARC-II observations and data reduction. We thank Andrew Blain for providing us with 350-μm number count predictions. We are also grateful to Jason Stevens and Nick Seymour for helpful suggestions. We thank the IRAC instrument team for allowing publication of GTO data on 4C 41.17. We also thank Mark Dickinson and Emily MacDonald for providing the DEIMOS/Keck z-band image of 4C 41.17. Some of the data presented herein were obtained at the W. M. Keck Observatory, which is operated as a scientific partnership among the California Institute of Technology, the University of California and the National Aeronautics and Space Administration. The Observatory was made possible by the generous financial support of the W. M. Keck Foundation. The authors wish to recognize and acknowledge the very significant cultural role and reverence that the summit of Mauna Kea has always had within the indigenous Hawaiian community; we are most fortunate to have the opportunity to conduct observations from this mountain. The work of DS was carried out at Jet Propulsion Laboratory, California Institute of Technology, under a contract with NASA.

REFERENCES

Archibald E. N., Dunlop J. S., Hughes D. H., Rawlings S., Eales S. A., Ivison R. J., 2001, MNRAS, 323, 417
Blain A. W., Smail I., Ivison R. J., Kneib J.-P., Frayer D. T., 2002, Phys. Rev., 369, 111
Benford D. J., Pierre C., Omont A., Phillips T. G., McMahon R. G., 1999, ApJ, 518, L65.
Best P. N., Longair M. S., Röttgering H. J. A., 1998, MNRAS, 295, 549
Bondi M. et al., 2003, A&A, 403, 857
Carilli C. L., Yun M., 1999, ApJ, 513, L13
Chambers K. C., Miley G. K., van Breugel W., Bremer M., Huang J.-S., Trentham N., 1996, ApJS, 106, 247
Chapman S. C., Scott D., Windhorst R. A., Frayer D. T., Borys C., Lewis G. F., Lvison R. I., 2004, ApJ, 606, 85
Chapman S. C., Blain A. W., Smail I., Ivison R. J., 2005, ApJ, 622, 772
Chini R., Krügel E., 1994, A&A, 288, L33
Condon J. J., 1984, ApJ, 287, 461
Condon J. J., 1992, ARA&A, 30, 575
Condon J. J., Cotton W. D., Greisen E. W., Yin Q. F., Perley R. A., Taylor G. B., Broderick J. J., 1998, AJ, 115, 1693
Coppin K. et al., 2006, MNRAS, 372, 1621
De Breuck C., van Breugel W., Röttgering H. J. A., Miley G., 2000, A&AS, 143, 303
De Breuck C., van Breugel W., Stanford S. A., Röttgering H. J. A., Miley G., Stern D., 2002, AJ, 123, 637
De Breuck C. et al., 2003, A&A, 401, 911
De Breuck C. et al., 2004, A&A, 424, 1
De Breuck C., Downes D., Neri R., van Breugel W., Reuland M., Omont A., Ivison R., 2005, A&A, 430, L1
Douglas J. N., Bash F. N., Bozyan F. A., Torrence G. W., Wolfe C., 1996, AJ, 111, 1945
Dowell C. et al., 2003, in Phillips T. G., Zmuidzinas J., eds, Proc. SPIE Vol. 4855, Millimeter and Submillimeter Detectors for Astronomy. SPIE, Bellingham WA, p. 73
Downes A. J. B., Peacock J. A., Savage A., Carrie D. R., 1986, MNRAS, 218, 31
Dunlop J. S., Hughes D. H., Rawlings S., Eales S. A., Ward M. J., 1994, Nat, 370, 347
Eales S., Bertoldi F., Ivison R. J., Carilli C. L., Dunne L., Owen F., 2003, MNRAS, 344, 169
Eckart M., Stern D., Helfand D., Harrison F., Mao P., Yost S., 2006, ApJS, 165, 19
Faber S. M. et al., 2003, in Iye M., Moorwood A. F. M., eds, Proc. SPIE Vol. 4841, Instrument Design and Performance for Optical/Infrared Ground-based Telescopes. SPIE, Bellingham WA, p. 1657
Fynbo J. P. U., Møller P., Warren S. J., 1999, MNRAS, 305, 849
Greve T. R., Ivison R. J., Papadopoulos P. P., 2004a, A&A, 419, 99
Greve T. R., Ivison R. J., Bertoldi F., Stevens J. A., Dunlop J. S., Lutz D., Carilli C. L., 2004b, MNRAS, 354, 779
Haiman Z., Rees M., 2001, ApJ, 556, 87
Haiman Z., Spaans M., Quataert E., 2000, ApJ, 537, L5
Hildebrand R. J., 1983, QJRAS, 24, 267
Hippelein H., Meisenheimer K., 1993, Nat, 362, 224
Hughes D. H., Dunlop J. S., Rawlings S., 1997, MNRAS, 289, 766
Hughes D. H. et al., 1998, Nat, 394, 241
Hooper E. J., Impey C. D., Foltz C. B., Hewett P. C., 1995, ApJ, 445, 62
Ivison R. J., 1995, MNRAS, 275, L33
Ivison R. J., Smail I., Le Borgne J.-F., Blain A. W., Kneib J.-P., Bezecourt J., Kerr T. H., Davies J. K., 1998, MNRAS, 298, 583
Ivison R. J., Dunlop J. S., Smail I., Dey A., Liu M. C., Graham J. R., 2000, ApJ, 542, 27
Ivison R. J. et al., 2002, MNRAS, 337, 1
Ivison R. J., Smail I., Dunlop J. S., Jenner C. E., 2002, in Lowenthal J. D., Hughes D. H., eds, Deep Millimeter Surveys: Implications for Galaxy Formation and Evolution. World Scientific, Singapore, p. 135
Ivison R. J. et al., 2004, ApJ, 154, 124
Ivison R. J. et al., 2005, MNRAS, 364, 1025
Ivison R. J. et al., 2007, MNRAS, 380, 199
John T. L., 1988, A&A, 193, 189
Johnson O., Best P. N., Almaini O., 2003, MNRAS, 343, 924
Kennicutt R. C., 1998, ApJ, 498, 541
Klamer I. J., Ekers R. D., Sadler E. M., Weiss A., Hunstead R. W., De Breuck C., 2005, ApJ, 621, L1
Kodama T., Tanaka I., Kajisawa M., Kurk J., Venemans B., De Breuck C., Vernet J., Lidman C., 2007, MNRAS, 377, 1717
Kovács A., 2006, PhD thesis, California Institute of Technology, http://etd.caltech.edu/etd/available/etd-06022006-123747
Kreysa E. et al., 1998, in Phillips T. G., ed., Proc. SPIE Vol. 3357, Advanced Technology MNW Radio, and Terahertz Telescopes. SPIE, Bellingham WA, p. 319
Kurk J., Röttgering H. J. A., Pentericci L., Miley G. K., Overzier R., 2003, New Astron. Res., 47, 339
Kurk J., Pentericci L., Röttgering H. J. A., Miley G. K., 2004, A&A, 428, 793
Lacy M. et al., 2004, ApJS, 154, 1
Lacy M. et al., 2005, ApJS, 161, 41
Miley G. K. et al., 2004, Nat, 427, 47
Oke J. B. et al., 1995, PASP, 107, 375
Ohyama Y. et al., 2003, ApJ, 591, L9
Papadopoulos P. P., Röttgering H. J. A., van der Werf P. P., Guilloteau S., Omont A., van Breugel W. J. M., Tilanus R. P. J., 2000, ApJ, 528, 626
Papovich C. et al., 2004, ApJS, 154, 70
Pentericci L. et al., 2000, A&A, 361, L25
Pentericci L., Kurk J. D., Carilli C. L., Harris D. E., Miley G. K., Röttgering H. J. A., 2002, A&A, 396, 109
Pope A. et al., 2006, MNRAS, 370, 1185
Rengelink R. B., Tang Y., de Bruyn A. G., Miley G. K., Bremer M. N., Röttgering H. J. A., Bremer M. A. R., 1997, A&AS, 124, 259
Reuland M. et al., 2003, ApJ, 592, 755
Reuland M., Röttgering H., van Breugel W., De Breuck C., 2004, MNRAS, 353, 377
Sawicki M., 2002, AJ, 124, 3050
Scott S. E. et al., 2002, MNRAS, 331, 817
Seymour N. et al., 2007, ApJS, 171, 353
Smail I., Ivison R. J., Kneib J.-P., Cowie L. L., Blain A. W., Barger A. J., Owen F. N., Morrison G., 1999, MNRAS, 308, 1061
Smail I., Ivison R. J., Owen F. N., Blain A. W., Kneib J.-P., 2000, ApJ, 528, 612
Smail I., Ivison R. J., Gilbank D. G., Dunlop J. S., Keel W. C., Motohara K., Stevens J. A., 2003a, ApJ, 583, 551
Smail I., Scharf C. A., Ivison R. J., Stevens J. A., Bower R. G., Dunlop J. S., 2003b, 599, 86
Spergel D. N. et al., 2003, ApJS, 148, 175
Steidel C. C., Adelberger K. L., Shapley A. E., Pettini M., Dickinson M., Giavalisco M., 2000, ApJ, 532, 170
Stern D., Djorgovski S. G., Perley R. A., de Carvalho R. R., Wall J. V., 2000, AJ, 119, 1526
Stern D. et al., 2005, ApJ, 631, 163
Stevens J. A. et al., 2003, Nat, 425, 264
Taniguchi Y., Shioya Y., 2000, ApJ, 532, L13
van Oijk R., Röttgering H. J. A., Miley G. K., Hunstead R. W., 1997, A&A, 317, 496
Venemans B. P. et al., 2007, A&A, 461, 823
Visnovsky K. L., Impey C. D., Foltz C. B., Hewett P. C., Weymann R. J., Morris S. L., 1992, ApJ, 391, 560
Voss H., Bertoldi F., Carilli C. L., Owen F. N., Lutz D., Holdaway M., Ledlow M., Menten K. M., 2006, A&A, 448, 823
Weidinger M., Møller P., Fynbo J. P. U., Thomson B., 2005, A&A, 436, 825
White R. L., Becker R. H., 1992, ApJS, 79, 331
Wilman R. J., Jarvis M. J., Röttgering H. J. A., Binette L., 2004, MNRAS, 351, 1109
Zylka R., 1998, Pocket Cookbook for the MOPSI Software, http://www.iram.es/IRAMES/mainWiki/CookbookMopsic

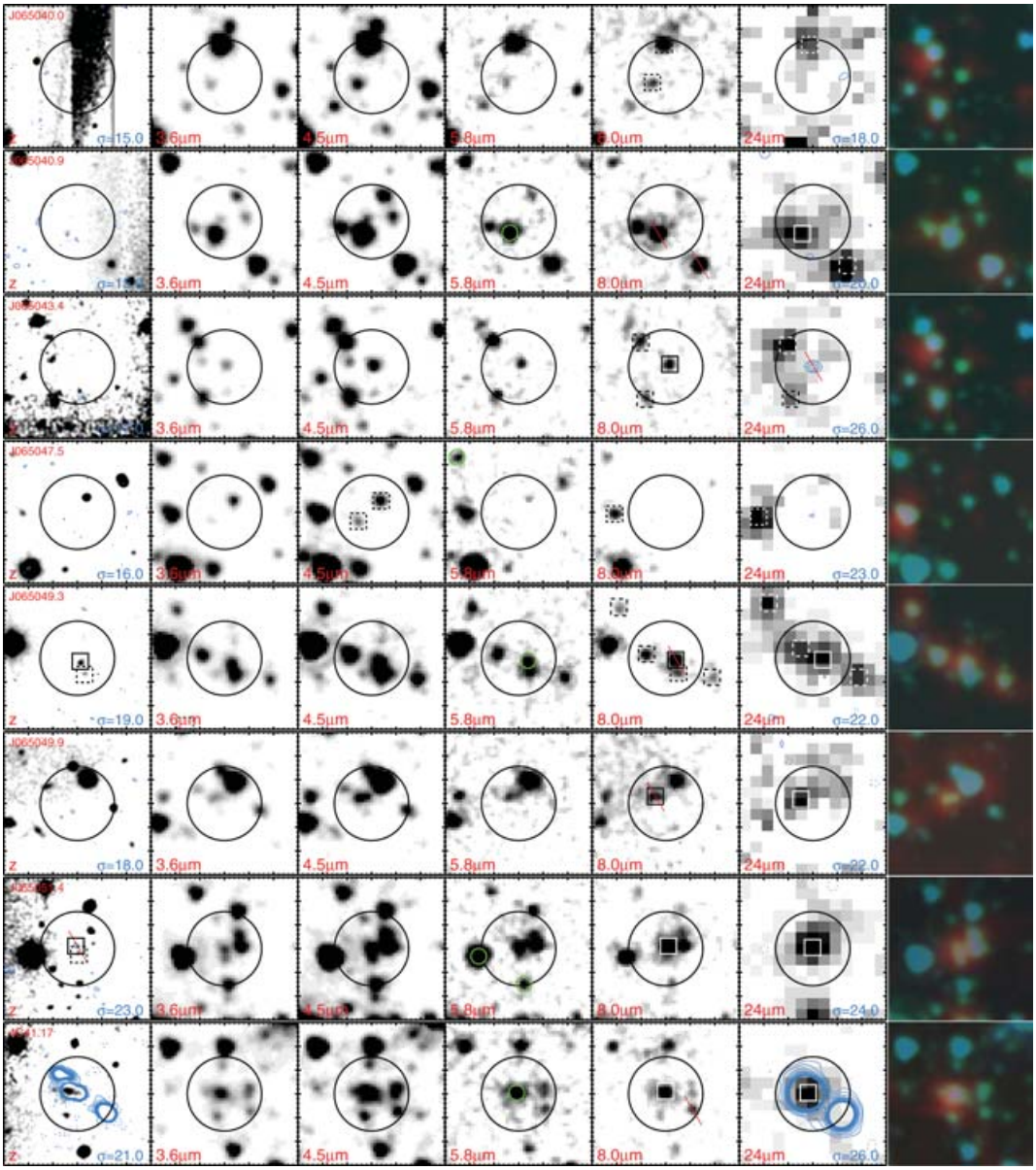

Figure A1. 30 × 30-arcsec^2 postage stamp images of the 14 SMGs (and 4C 41.17) detected towards 4C 41.17. The postage stamp images are centred on the (sub)mm centroid. Although, in cases where a source was detected at more than one (sub)mm wavelength, the postage stamp image has been centred on the average (sub)mm centroid (Table 3). The leftmost column shows z-band images (grey-scale) with radio 1.4-GHz contours overlaid. The radio contours are plotted at -3, 3, 4, . . .10, 20. . . 100σ, where σ is the local rms noise. The middle five columns (from the left-hand to right-hand side) show grey-scale images at 3.6, 4.5, 5.8 and 8.0 μm (IRAC) and 24 μm (MIPS). The latter with 4.9-GHz radio contours overlaid at -3, 3, 4. . .10, 20. . .100σ, where σ is the local rms noise. The solid central circle indicates the 8-arcsec error circle within which we have searched for radio and mid-IR counterparts. The solid squares indicate robust identifications (i.e. $P \leqslant 0.05$) based on radio or 24-μm counts, while the dashed squares indicate possible counterparts. The red lines represent the position of slits on our LRIS masks and the green circles represent X-ray sources detected with *Chandra* (Smail et al. 2003b). The last column shows the 'true' colour postage stamp images, based on the 3.6-μm (blue), 4.5-μm (green) and 24-μm (red) images.

APPENDIX A: NOTES ON INDIVIDUAL SOURCES

(i) *J065040.0.* A radio-blank field containing two possible mid-IR counterparts. One is detected in the IRAC bands only and is located 3 arcsec south-east of the SMG position. The other, located about 7 arcsec north of the (sub)mm centroid, is also strongly detected in the near-IR and at 24 μm. The likelihood of either source being a chance association is non-negligible, however, and we are therefore unable to unambiguously identify the correct near-/mid-IR counterpart for this SMG.

(ii) *J065040.9.* A radio-blank field, but several possible counterparts are seen in the IRAC bands. The two brightest 8.0-μm sources coincide with an extended, apparently blended 24-μm source about 5 arcsec south-east of the (sub)mm centroid. The 24-μm peak, however, coincides with the brightest IRAC source suggesting that most of the 24-μm emission comes from this source. Invoking the findings by Pope et al. (2006) that in most cases where multiple 24-μm sources are found within a SCUBA beam, only one – namely the brightest 24-μm source – is dominating the submm emission, it would suggest that this source is the counterpart to the SMG. This

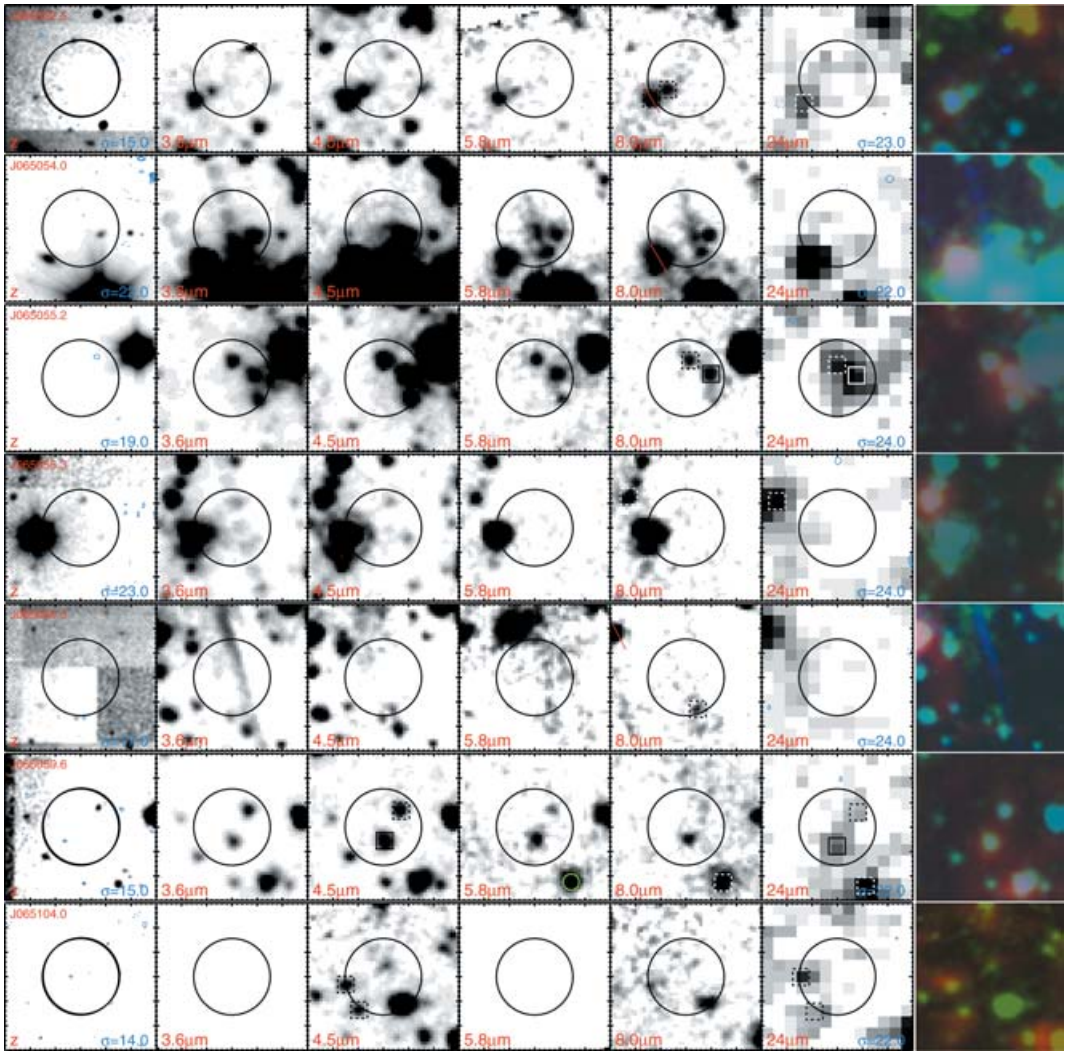

Figure A1 – *continued*

is further strengthened by the fact that the source also has an X-ray counterpart detected by *Chandra*. We find the 24-/1200-μm association to be statistically significant ($P < 0.029$). The IRAC source was targeted spectroscopically but due to its faintness in the near-IR and the poor quality of the spectrum we were unable to infer a redshift. The spectrum of a second 24-μm source lying 11.5 arcsec to the south-west of the mm centroid yielded a redshift of $z = 0.909 \pm 0.002$. This source, however, is not a statistically significant counterpart.

(iii) *J065043.4.* Two 24-μm sources are found at the edge of the error circle, but neither of them is a statistically robust counterpart (see Table 4). However, a statistically significant mm/radio association ($P = 9 \times 10^{-5}$) is obtained for the robust (4.5σ) 4.9-GHz source ($S_{4.9\,\mathrm{GHz}} = 109.2 \pm 31.1$ μJy) near-coincident with the 1200-μm centroid. The radio source, which appears to be unresolved, coincides with a point source detected in all the IRAC bands, but no counterpart is seen either in the z band or at 24 μm. Based on the strong 4.9-GHz radio ID, we adopted this source as the radio/mid-IR counterpart to J065043.4 and it was subsequently targeted with LRIS. The resulting spectrum is shown in Fig. A2(a): strong Lyα emission, extended on scales of 13.2 arcsec, is detected at a wavelength corresponding to $z = 2.672 \pm 0.001$.

(iv) *J065047.5.* A strong 24-μm source is located ∼11 arcsec east of the mm centroid, but does not represent a statistically significant identification. Two IRAC sources are found within the positional error circle of this radio-blank field, but neither source is associated with any 24-μm emission and their association with the SMG is not significant. Thus, the correct mid-IR/radio counterpart for this source is undetermined.

(v) *J065049.3.* Two faint z-band sources, separated by ∼2.7 arcsec, and their matching counterparts in the IRAC channels are detected near the centre of the error beam. The two sources (K1 and K2) were initially suggested as near-IR counterparts to the SMG by Ivison et al. (2000) on the basis of their resolved 850-μm emission (see fig. 1 of Ivison et al. 2002b) – with K1 denoting the source closest to the centre. K1 is the reddest, while K2 becomes fainter and more extended in the long-wavelength IRAC channels. In the 24-μm MIPS band, the two sources, together with an IRAC source ∼5 arcsec west of the centre, combine into a single, blended source. We note that K1, apart from being the reddest IRAC source and the only X-ray source within the error circle, also coincides with the peak of the (blended) 24-μm emission. This peak is dominating the total flux, thus making it the most likely mid-IR counterpart to the submm emission. In fact, we find a statistically significant

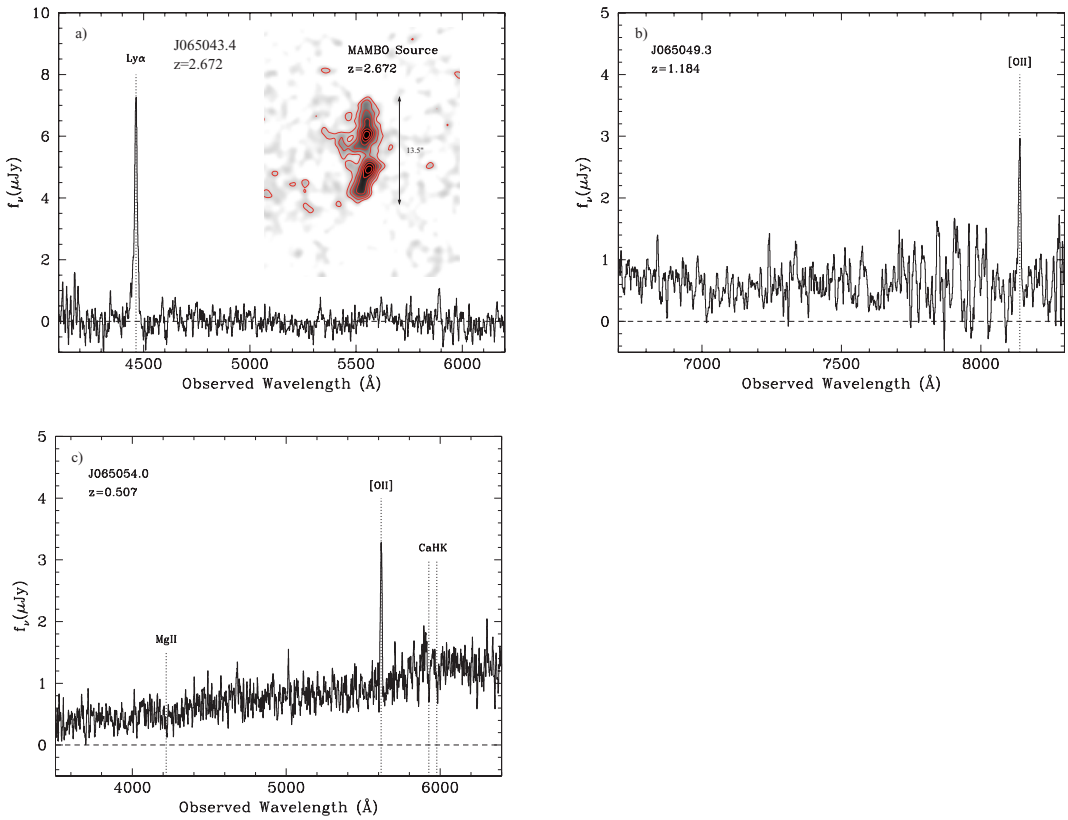

Figure A2. Keck/LRIS spectra of J065043.4 (a), J065049.3 (b) and J065054.0 (c). The inset grey-scale 2D spectrum in (a) shows the extended Lyα emission associated with J065054.0. The spatial axis is vertical and the spectral axis is horizontal.

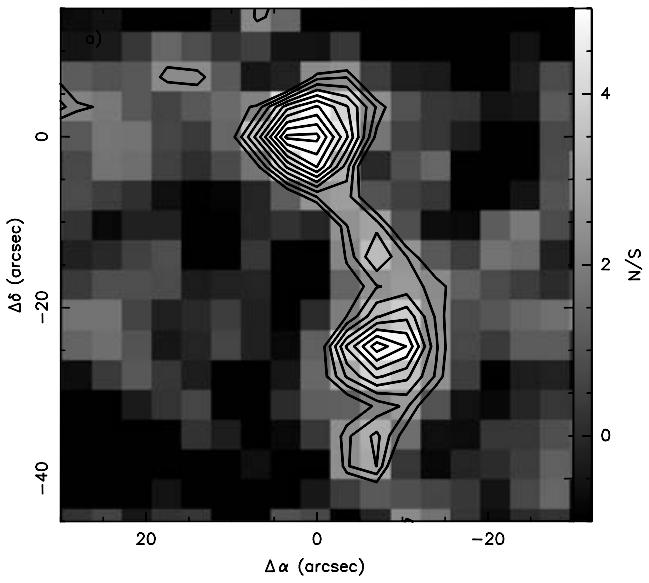

Figure A3. A zoom-in of the inner 30 × 30-arcsec^2 region around 4C 41.17 and J065051.4 in the 1200-μm S/N map. Contours are at S/N = 2.0, 2.5, 3.0, . . ., 8.0.

1200-/24-μm association ($P = 0.011$) for K1. Moreover, LRIS spectroscopy of K1 yields a redshift of $z = 1.184 \pm 0.002$ (Fig. A2b), which is within the redshift distribution of blank-field SMGs (Chapman et al. 2005), thus further suggesting that this is the correct counterpart. It is possible, however, that K1 is part of a composite system which includes the bluer component K2. From the estimated 24-μm flux of the third IRAC source within the error beam (Table 4), we find this to be a non-significant 24-μm/mm association ($P = 0.067$). Further two 24-μm sources are found 15.0 arcsec south-west and 10.5 arcsec north-east of the mm centroid – but neither qualifies as a robust counterpart. Thus, we conclude that K1 is the correct near-/mid-IR counterpart to J065049.3 with K2 being a possible associated system.

(vi) *J065049.9*. While no radio sources are detected within 8 arcsec of the 1200-μm centroid, at least five IRAC sources are found within the search radius. The reddest [$\log(S_{5.8\,\mu m}/S_{3.6\,\mu m}) = -0.045$] IRAC source, which is also the one closest to the mm centroid, coincides with a robust 24-μm source. The latter constitutes a robust 1200-/24-μm association ($P = 0.012$) and we take this source to be the mid-IR counterpart to J065049.9. LRIS spectroscopy of this source did not yield any discernable lines/continuum.

(vii) *J065051.4*. An unambiguous mm/radio association ($P = 0.002$) is found from the 1.4-GHz map which shows a robust source at RA: 06:50:51.4 and Dec.: +41:30:06.5, that is, within ∼1 arcsec of the 1200-μm centroid. The radio source coincides with the reddest [$\log(S_{5.8\,\mu m}/S_{3.6\,\mu m}) = 0.23$] and northernmost component of a slightly blended IRAC source as well as with a robust 24-μm point source ($S_{24\,\mu m} = 448 \pm 24$ μJy). The latter yields a robust 1200-/24-μm association ($P = 0.002$). A faint z-band source is seen just ∼1 arcsec south of the radio source. This source is also detected at 3.5 and 4.5 μm where it appears to be interacting with the radio-identified IRAC source. Given their proximity and merger-like appearance, it is tempting to speculate that both sources are part of the same system. Unfortunately, the optical LRIS spectrum, obtained with a slit at the radio position, did not yield any

identifiable line or continuum emission; we are therefore unable to infer a spectroscopic redshift for this source. At a resolution of 3.1 $\times$ 2.3 arcsec^2, continuum observations at 1.3 mm of this source with the IRAM Plateau de Bure Interferometer (PdBI) failed to yield a detection ($3\sigma \lesssim 2.2$ mJy) (D. Downes, private communications). The blank IRAM PdBI image implies that the (sub)mm emission is spread over a large area or breaks down into two or more fainter components. Based on present data the evidence is ambiguous, although there may be some support for the latter scenario looking at Fig. A3 where we have zoomed in on a 30 $\times$ 30-arcsec^2 region around 4C 41.17 and J065051.4. Contours at the 2–3σ level show evidence of faint emission extending between the two sources as well as the presence of two faint sources north and south of J065051.4.

(viii) *4C 41.17.* The two radio lobes and the radio galaxy itself are evident from the 1.4-GHz radio contours. The radio galaxy coincides with the (sub)mm centroid and is clearly detected in the z, IRAC and 24-μm bands as well as in the X-rays. The south-western radio lobe coincides with a faint source detected in the IRAC bands. This source was first detected at 2.15 μm (K_s band) by Papadopoulos et al. (2005) who speculated that it could be due to jet-induced star formation. The source was targeted spectroscopically but unfortunately neither discernable line nor continuum emission was detected.

(ix) *J065052.5* A radio-blank field, in which a robust 24-μm source is seen ∼9 arcsec to the south-east of the mm centroid, just outside the positional error circle. It does not, however, represent a significant 24-μm/mm association ($P = 0.084$). The LRIS spectrum of this source spectrum did not yield any discernable emission lines. An IRAC source about 5 arcsec south-east of the mm centroid, which coincides with extremely faint z-band emission but is undetected at 24 μm, is another possible, but not statistically significant, counterpart. The radio/mid-IR identification of this SMG therefore remains ambiguous.

(x) *J065054.0.* No robust radio sources are detected in this field. Three IRAC sources lie within the 8-arcsec search circle, neither of which qualifies as a robust counterpart to the SMG. However, a strong 24-μm source ∼9 arcsec south-west of the mm centroid is a statistically significant mid-IR 24-/mm association ($P = 0.043$). Even though this source lies (just) outside the 8 arcsec search radius, we still adopt it as the correct 24-μm counterpart. In the z band, the source appears as a lenticular galaxy. The Keck/LRIS spectrum of this source is shown in Fig. A2(c) and we infer a spectroscopic redshift of $z = 0.507 \pm 0.002$.

(xi) *J065055.2.* Bright, extended 24-μm emission is found within the 8 arcsec search radius in this radio-blank field. In the IRAC bands, this emission is resolved into three separate sources. The bulk of the 24-μm emission coincides with the brightest IRAC source located ∼2.9 arcsec north-west of the mm centroid, and we find the probability of this being a non-random association to be statistically significant ($P = 0.031$). We have estimated the contribution to the 24-μm emission by the two other IRAC sources and find that they both fall short of being a robust 24-μm/mm association.

(xii) *J065055.3.* A radio-blank field which is also hard to interpret in the mid-IR. A bright 24-μm source lies ∼14 arcsec north-east of the mm centroid but does not make the cut as a robust counterpart ($P = 0.098$). Two very faint z-band sources are detected ∼6 arcsec north and ∼3 arcsec south-west of the SMG centroid. Both sources have weak counterparts in the 3.6- and 4.5-μm IRAC channels, but elude detection at 5.8 and 8.0 μm as well as at 24 μm. Neither source represents a significant mid-IR/mm association, and the correct counterpart for this SMG therefore remains elusive.

(xiii) *J065059.3.* A radio-blank field. A faint, morphologically complex IRAC source ∼7 arscec south-west of the SMG position is the only source found within the 8 arcsec search radius. It is detected neither at 24 μm nor in the near-IR, and it does not constitute a statistically significant mid-IR/mm association. Thus, we are not able to assign a robust mid-IR identification to this SMG.

(xiv) *J065059.6.* A robust 24-μm source peaks ∼4 arcsec south of the mm centroid and makes up a statistically significant 24-μm/mm association ($P = 0.048$). The source coincides with an IRAC source with a slightly extended appearance. Extremely faint 24-μm emission is located ∼6 arcsec to the north-west of the centre via its IRAC and z-band counterparts, while a bright, X-ray detected 24-μm source is seen ∼14.8 arcsec from the centre. However, neither of these two sources constitutes an unambiguous identification.

(xv) *J065104.0.* Guided by the IRAC images, two faint 24-μm source are found ∼9 arcsec east and south-east of the mm centroid. However, neither source is a robust counterpart ($P = 0.078$ and $P > 0.1$, respectively) and the correct identification therefore remains ambiguous.

This paper has been typeset from a TEX/LATEX file prepared by the author.